MASARYKOVA UNIVERZITA
Přírodovědecká fakulta
Ústav teoretické fyziky a astrofyziky

Rentgenová spektroskopie horkého plynu obklopujícího masivní rotující galaxii

Bakalářská práce

Anna Juráňová

Vedoucí práce: doc. Mgr. Norbert Werner, Ph.D. **Brno 2017**

Bibliografický záznam

Autor:	Anna Juráňová Přírodovědecká fakulta, Masarykova univerzita Ústav teoretické fyziky a astrofyziky
Název práce:	Rentgenová spektroskopie horkého plynu obklopujícího masivní rotující galaxii
Studijní program:	Fyzika
Obor:	Astrofyzika
Vedoucí práce:	doc. Mgr. Norbert Werner, Ph.D.
Akademický rok:	2016/2017
Počet stran:	ix + 50
Klíčová slova:	čočkovité galaxie, aktivní galaxie, rentgenová spektroskopie, horký plyn

Bibliographic record

Author:	Anna Juráňová Faculty of Science, Masaryk University Department of Theoretical Physics and Astrophysics
Title of Thesis:	X-ray spectroscopy of hot gas surrounding a massive fast rotating galaxy
Degree Programme:	Physics
Field of study:	Astrophysics
Supervisor:	doc. Mgr. Norbert Werner, Ph.D.
Academic Year:	2016/2017
Number of Pages:	ix + 50
Keywords:	lenticular galaxies, active galaxies, X-ray spectroscopy, hot gas

Abstrakt

Pozorování v delších vlnových delkách spolu s teoretickými modely horkého plynu ve hmotných galaxiích raného typu předpovídají odlišné chování systémů s nezanedbatelným momentem hybnosti ve srovnání s těmi nerotujícími, a to díky účinkům rotace na stabilitu plynu. V této práci prezentujeme měření horkého plynu čočkovité galaxie NGC 7049 získané družicí XMM-Newton. Spektrální vlastnosti tohoto objektu umožnily naměření systematicky vyšší míry entropie, než jaká je běžná u galaxií bez jednotného smyslu rotace, které jako NGC 7049 obsahují chladný plyn v centrální oblasti. V sektorech zahrnujících emisi plynu geometricky blízkého tomu atomárnímu v rovině rotace byly detekovány známky přítomnosti multiteplotního plazmatu, naznačujícího probíhající chladnutí horké složky. Z vlastností horkého plynu usuzujeme, že jeho rotace pravděpodobně je schopná podpořit rozvoj chladnutí v podmínkách, které by k takovým procesům v galaxiích s nulovým celkovým momentem hybnosti nevedly.

Abstract

Observations from longer wavelengths along with theoretical models of hot gas permeating massive early-type galaxies suggest different behaviour of objects with significant net angular momentum due to rotational support additional to buoyancy. Analysing spectroscopic measurement from XMM-Newton of X-ray emitting gas in lenticular galaxy NGC 7049, we determined systematically higher entropy throughout the galaxy compared to non-rotating systems possessing cold gas in their centres. We detected indication for multitemperature plasma in the plane of rotation, more specifically in region containing dusty cold disk near central part of the galaxy, suggesting a possibility of ongoing cooling from the hot phase. We conclude that rotational support of the hot gas is likely capable of enhancing the development of thermal instabilities leading to cooling onto a non-radial orbit, despite otherwise unsuitable conditions when measured in non-rotating galaxies.

MASARYKOVA UNIVERZITA
Přírodovědecká fakulta

ZADÁNÍ BAKALÁŘSKÉ PRÁCE

Akademický rok: 2016/2017

Ústav: Ústav teoretické fyziky a astrofyziky

Studentka: Anna Juráňová

Program: Fyzika

Obor: Astrofyzika

Ředitel *Ústavu teoretické fyziky a astrofyziky* PřF MU Vám ve smyslu Studijního a zkušebního řádu MU určuje bakalářskou práci s názvem:

Název práce: Rentgenová spektroskopie horkého plynu obklopujícího masivní rotující galaxii

Název práce anglicky: X-ray spectroscopy of hot gas surrounding a massive fast rotating galaxy

Oficiální zadání:
Observations of massive cooling core clusters and of giant elliptical galaxies indicate that the cold gas in these systems may be produced chiefly by cooling from the hot phase. Recently, there have been considerable numerical and theoretical efforts to study thermally unstable cooling. The properties of cooling in the presence of significant angular momentum are, however, likely to be different from cooling in non-rotating atmospheres. The student will analyze new X-ray data, obtained by the XMM-Newton satellite, of NGC 7049, a nearby (d = 29.9 Mpc) giant elliptical/S0 central group galaxy with a rotating disk of dusty cold gas. The student will determine the morphology and thermodynamic properties of the hot X-ray emitting atmosphere of the galaxy and will test predictions for cooling instabilities in systems with significant angular momentum, such as cooling from the X-ray emitting phase, the presence of an elongated rotating X-ray emitting atmosphere, and inefficient AGN heating close to the plane of the disk. The study will inform our understanding of the role of cooling instabilities in the process of galaxy formation and evolution.

Jazyk závěrečné práce: angličtina

Vedoucí práce: doc. Mgr. Norbert Werner, Ph.D.

Datum zadání práce: 7. 11. 2016

V Brně dne: 21. 4. 2017

Souhlasím se zadáním (podpis, datum): 26. 4. 2017

Anna Juráňová **studentka**	doc. Mgr. Norbert Werner, Ph.D. **vedoucí práce**	prof. Rikard von Unge, Ph.D. **ředitel Ústavu teoretické fyziky a astrofyziky**

Poděkování

I would like to express my sincere gratitude to my supervisor doc. Mgr. Norbert Werner, Ph.D. for his immense knowledge, encouragement, limitless patience, and guidance throughout this work. Besides my supervisor, many thanks belong to Mgr. Filip Hroch, Ph.D. for the priceless advice and support he has given me and to Kiran Lakhchaura for her valuable help with deprojection.

I am also very grateful for the possibility of participating in training lead by experts in X-ray astronomy and XMM-Newton issues in Netherlands Institute for Space Research SRON via funding of AHEAD Trans-National Access.

Prohlášení

Prohlašuji, že jsem svoji bakalářskou práci vypracovala samostatně s využitím informačních zdrojů, které jsou v práci citovány.

Brno 16. května 2017

Podpis autora

Contents

Introduction

Ever since were the galaxies established as systems like the Milky Way, they triggered the attention of astronomers, who aspired for explaining their formation, interactions and various structures. Soon, the galaxies were distinguished by their shape and the most natural division was firmly established in form of the 'Hubble fork', giving rise to straightforward names: elliptical, spiral, and lenticular galaxies, the latter providing a natural transition between the first two.

With advance of technology, it became clear that these distinguishable morphological structures are formed by numerous complicated processes operating at once – among others the composition of stellar populations, star formation rate, global dynamical properties, amount of cold gas and dark matter, and the violent processes in galactic centres.

It is well-known that galaxy clusters are filled with hot gas reaching up to tens of millions kelvins, controlled by massive black holes residing in centres of the brightest cluster galaxies. The same applies in reduced scale to other smaller, but still massive systems – groups and isolated galaxies – the precise mechanism is, however, elusive. Rotational support in galaxies might be one of the factors having the greatest impact on properties of the hot gas. Therefore, we focused on a lenticular galaxy, a fast rotating system, possessing an active nucleus and an extensive halo of hot gas. We examine the galaxy in X-rays, taking advantage of powerful X-ray spectroscopy in order to put constraints on ongoing processes leading to the formation of observable properties of the galaxy.

Chapter 1

Hot gas in elliptical and lenticular galaxies

What dominates the luminosity of giant elliptical (E) and lenticular (S0) galaxies, together known as early-type galaxies, in the optical part of the spectrum and what has for a long time been the only indicative of baryonic mass, is the emission of stellar photospheres. However, energetic baryons permeating the galaxies and even extending beyond their boundaries by far dominate the high energy band.

The mass of the hot gas $M_{\rm gas}$ reaches up to $10^{10}\,M_{\odot}$, which is about $2\,\%$ of the mass of stellar component. Having temperatures of $10^6 - 10^7\,\mathrm{K}$, its presence can be revealed in X-ray part of the spectra. In the following sections, its origin, physical properties, and ongoing processes are discussed.

1.1 Origin of the hot gas

Generally, two main sources of hot gas in galaxies exist. Internal source constitutes mainly of stellar mass loss, which contributes to the overall gas mass at a rate $\sim 1.3[L_{\rm B}/(10^{11}\,L_{\rm B,\odot})]\,M_{\odot}\,\mathrm{yr}^{-1}$ in ellipticals, which is also applicable to S0s. It is assumed that the ejected gas heats up by passing through shocks and gains stellar kinematic temperature $T_{\star} \approx T_{\rm vir} \approx \mu m_{\rm p}\sigma^2/k \sim 10^7\,\mathrm{K}$, where μ is molecular weight and σ is the stellar velocity dispersion. Along with red giants, to which the stellar mass loss applies the most, supernovae (SNe) type Ia also contribute to the gas reservoir. As the star formation rate is generally low for both E and S0, type II supernovae do not occur any more due to requirements on their progenitors. On the other hand, during formation of the galaxy when the star formation rate was much higher, core collapse SNe were also more frequent and thus enriched the surrounding environment (Mathews and Brighenti, 2003) of galaxies out of their farthest peripheries. This outer reservoir serves as a part of the second – external – source, as the gas falls back into the potential well of its progenitor. Particles are shock-heated during their entrapment to the virial temperature of the galaxy (or group/cluster). Build-up of both stellar and gas mass is significantly enlarged by merging satellite systems and other galaxies (Bell et al., 2004; Faber et al., 2007).

1.2 Basic physical properties

Description of the highly ionised X-ray plasma permeating galaxies and galaxy clusters takes advantage of several simplifying approximations based on studies of the Solar Corona, the coronal approximation (Elwert, 1952). In the coronal model, the plasma is assumed to be optically thin, so that X-rays do not influence populations in the bound atomic levels and are not affected by the medium themselves. This is valid for low radiation density which is present in galactic atmospheres.

Another assumption concerns radiative losses and expects them to be balanced by non-radiative heating, that includes heating in magneto-hydro-dynamic waves or shock waves. Next, both electrons and ions are expected to be locally relaxed to Maxwellian energy distribution with common temperature and in statistical equilibrium for ionisation balance and bound atomic states (Mewe, 1999). This is achieved when the time needed for the plasma is long enough for particles to share their energy. If these conditions are met, the plasma is regarded to be in collisional equilibrium.

There are cases, however, in which the situation is quite different. Thermally unstable regions may spring up in central parts of the gas, each at a different, but locally common temperature. Simple single temperature models would then not be able to describe the spectrum. (Peterson and Fabian, 2006)

1.3 Cooling flows

A significant part of the observed X-ray radiation of the gas permeating the galaxy does not result in a proportional decrease of the temperature. Instead, this loss of energy is compensated by its gain in compression by the gravitational potential that maintains the virial temperature T_{vir} of the gravitating object. However, in central regions of the galaxy, radiative cooling is allowed by the previous condition, since the potential does not decrease in any direction (Mathews and Brighenti, 2003) and particle number densities are sufficiently high, and creates a cooling flow. The gas there is subjected to a subsonic inflow, particle density increase and subsequently a further cooling, allowed by frequent Coulomb interactions of highly ionised particles with free electrons. Inward motion is demanded to support the weight of overlying gas by rising density in colder core.

Integral over gas emission weighted by the energy of the photons, shortly a cooling function or Λ, has a key role in determining the process of cooling taking into account present elemental abundances. It is defined as

$$\Lambda(T, Z_i) = \int_0^\infty E \,\frac{\mathrm{d}\alpha(E, T, Z_i)}{\mathrm{d}E}\,\mathrm{d}E, \tag{1.1}$$

where $\mathrm{d}\alpha/\mathrm{d}E$ is the energy dependent line (or continuum) power. Dependence of Λ on both temperature and abundances is described in Schure et al. (2009).

Relative distribution of temperatures in plasma is often conveniently expressed by means of an emission measure distribution. The differential emission measure $\mathrm{d}Y/\mathrm{d}T$ is defined as a multiplicative factor in an integrand of an energy-dependent emissivity as follows.

$$\frac{\mathrm{d}\epsilon}{\mathrm{d}E} = \int_0^\infty \frac{\mathrm{d}Y}{\mathrm{d}T} \frac{\mathrm{d}\alpha(E,T)}{\mathrm{d}E}\,\mathrm{d}T \tag{1.2}$$

This relation leads us towards the definition of a cooling time t_{cool}. A few approaches to the estimate of time required for the gas to cool completely can be found in literature, f.e. in work of Peterson and Fabian (2006); Böhringer and Werner (2010); Werner et al. (2010) or Longair, p. 111. Here, we adopt the definition used also in Werner et al. (2010).

The cooling time of an optically-thin plasma is set to be the gas enthalpy over energy loss per unit volume. Since the enthalpy is $\frac{5}{2}nk_{\mathrm{B}}T$, the relation can be written as

$$t_{\mathrm{cool}} = \frac{\frac{5}{2}(n_{\mathrm{e}} + n_{\mathrm{i}})k_{\mathrm{B}}T}{n_{\mathrm{e}}n_{\mathrm{i}}\Lambda(T)}, \tag{1.3}$$

where n_{e} and n_i is electron and ion number density, respectively, and $n_i = 0.92n_{\mathrm{e}}$. The reason for using enthalpy of the plasma per unit volume instead of its thermal energy per volume lies in the conditions of the cooling process. As the gas cools and descends to the inner parts of the galaxy, its density raises to maintain the pressure and that leads to an increase of the heat capacity by a factor of 5/3 (Peterson and Fabian, 2006).

Putting typical values of the gas density, temperature and cooling function into the equation, we obtain a time which is surely less than the age of the universe t_{H}. In other words, with no source of heating the gas would have had sufficiently much time to cool down.

$$t_{\mathrm{cool}}/t_{\mathrm{H}} \approx \left(\frac{T}{10^8\,\mathrm{K}}\right)\left(\frac{10^{-2}\,\mathrm{cm}^{-3}}{n}\right)\left(\frac{10^{-23}\,\mathrm{erg\,cm^3\,s^{-1}}}{\Lambda}\right) < 1 \tag{1.4}$$

A steady, so called standard cooling flow can be expressed by a rate at which cooled mass is being deposited,

$$\dot{M} \backsimeq \frac{M_{\mathrm{gas}}}{t_{\mathrm{cool}}} = \frac{L_{\mathrm{X}}}{\frac{5}{2}k_{\mathrm{B}}T}\mu m_{\mathrm{H}}, \tag{1.5}$$

where L_{X} is total X-ray luminosity and the t_{cool} is expected to be equal to the inflow time (Nulsen et al., 1984). Here, for consistency with already mentioned quantities, we can rewrite L_{X} using differential emission measure

$$\frac{\mathrm{d}L}{\mathrm{d}T} = \frac{\mathrm{d}Y}{\mathrm{d}T}\Lambda(T) \tag{1.6}$$

to get a relation between the $\mathrm{d}Y/\mathrm{d}t$ and mass deposition rate $\dot{M}$ used in spectral modelling later on.

$$\frac{\mathrm{d}Y}{\mathrm{d}T} = \frac{5}{2}\frac{\dot{M}k}{\mu m_{\mathrm{H}} \Lambda(T)} \tag{1.7}$$

The reader should keep in mind that this formula only applies to an isobaric cooling flow and that the continuous compression of gas does not necessarily hold to all physically reachable scenarios. For example, if the gas was magnetically supported and therefore prevented from contracting, it would be subjected to isochoric cooling (and the factor in (1.7) would reduce to 3/2) (Peterson and Fabian, 2006).

The cooling flow should result in speed up of the star formation in central regions of the galaxies, when a significant amount of gas is present at temperatures low enough. And yet this has proven not to be generally observable neither in elliptical nor lenticular galaxies, which should along with X-ray emission show traces of newly created stars in optical band – instead, they *mostly* appear 'red and dead'.

Another question arises when the initial motion of gas cooling at large distances from the galactic core is taken into account. Overall motion of the gas should show correlation with stellar dynamics, which would support evidence of its origin in stellar mass-loss. This can be however violated by merger events or distortion of hydrostatic equilibrium due to strong AGN activity which would trigger mixing. In the majority of cooling systems, cold gas emission does not possess disk-like morphology, that would suggest conservation of angular momentum of in-falling matter. This can either be explained by no initial uniformity in motion, or that the angular momentum is dissipated in turbulence if the contracting flow rotates. (Nulsen et al., 1984)

Conservation of angular momentum in the gravitational potential of spherical symmetry would cause the gas to flatten onto circular orbit and the inflowing particles would deposit the angular momentum in an increase of radius of the excretion disc.

1.4 AGN heating

As has been proven, cores of massive galaxies harbour supermassive black holes (SMBH). Their activity is governed by accretion of matter and is reflected in giant structures observable in multiple spectral bands across the universe. The role of these objects – active galactic nuclei or simply AGN – seem to be vital for stabilising thermal processes in their maternal galaxies as a whole, in groups, and even galaxy clusters, spanning over several megaparsecs. Processes in the close vicinity, relative to the vast extra-/galactic structures, of the event horizon are amongst the most energetic ones and serve as powerful probes of complex theories, aiming to describe the laws of physics beyond limits of human imagination. These set on the transfer of energy from cores to outer regions which irreplaceably contributes to the deposits of the hot gas that radiates its energy towards potential observers.

Several common features are observed in scales from giant ellipticals up to galaxy clusters, and despite not being well pronounced in many cases, they are believed to play a crucial role in supporting observed small cooling rates, if present.

1.4.1 Cavities

Accretion of cold gas onto SMBH can generate powerful jets uplifting matter in collimated cones at relativistic velocities, extending into radio-bright lobes as observed f.e. in relatively close M87, the central giant E of Virgo cluster (Forman et al., 2005). Generated by these outbursts, cavities filled with low-density hot gas rise from central parts subsonically later on, therefore not creating shock fronts (Churazov et al., 2001; Reynolds et al., 2001), and stay in a pressure balance between cavities and the surrounding environment. As they move to greater radii, adiabatic expansion takes place to maintain the pressure equilibrium. Sizes of these features therefore vary greatly: diameters of $1 - 200\,\mathrm{kpc}$ have been detected, noting that smaller ones are far more frequently observed, and there is a convincing evidence for numerous cavities in one system being relatively common. However, the detection demands high-quality X-ray data of galactic atmospheres, especially when dealing with projection effects in case of cavities far from the plane of the sky. (McNamara and Nulsen, 2007)

The upward motion of the buoyant cavity causes the X-ray emitting gas to fill the newly created vacancy transferring the gravitational potential energy into the corresponding amount of kinetic energy. Assuming surrounding gas to be close to the hydrostatic equilibrium ($\rho g = -\mathrm{d}p/\mathrm{d}r$), the potential energy released as the cavity rises a distance δr is

$$\delta U = Mg\,\delta r = V\rho g\,\delta r = -V\frac{\mathrm{d}p}{\mathrm{d}r}\,\delta r = -V\delta p, \tag{1.8}$$

where $M = V\rho$ is a mass of the surrounding gas of density ρ displaced by the cavity of volume V. The change in pressure of the surrounding gas over δr is $\delta p = (\mathrm{d}p/\mathrm{d}r)\,\delta r$ and is used in the last equality. Because of the formerly stated condition of subsonic motion, the change of pressure in surrounding environment can be regarded as equally experienced by the gas filling the cavity. With negligible radiative losses, this change is an adiabatic process and thus entropy of the cavity remains constant. With the first law of thermodynamics expressed in terms of the enthalpy $\mathrm{d}H = T\mathrm{d}S + p\,\mathrm{d}V$, here $\mathrm{d}H = p\,\mathrm{d}V$, from the equation 1.8 it can immediately be seen that the kinetic energy increase of the ambient gas the cavity initiated at the expense of its enthalpy.

Total enthalpy of the cavity can be expressed by means of pV, the work required for inflation, using ratio of specific heat $\varGamma$ to cover thermal energy of the cavity, resulting in $H = \varGamma/(\varGamma - 1)pV$. For non-relativistic gas, $\varGamma = 5/3$

and $H = 2.5\,pV$, relativistic case with $\Gamma = 4/3$ then gives $H = 4\,pV$. Presence of magnetic field would put the lower boundary to only $H = 2pV$. The kinetic energy transmitted by upward directed motion is then dissipated due to viscosity, either in laminar or turbulent motion. (McNamara and Nulsen, 2007; Churazov et al., 2001)

1.4.2 Weak shocks

Even some strong shocks (entropy generating waves that cause a transition from supersonic to subsonic flow (Rosswog and Brüggen, 2007)) have been observed in extended X-ray emission of galaxies and clusters, it is expected that weak shocks outnumber them greatly, as evidence in favour of their presence despite the visibility difficulties has been found, leaving NGC 4636 as an example (Baldi et al., 2009).

In AGN outbursts, amounts of energy can be deposited into weak shocks, that, rather than supporting heating, slow down the cooling by increasing total energy of the gas to be radiated away and lower density of the gas which has a direct impact on the cooling rate. The key part in heating by weak shocks are inhomogeneities, more precisely cavities in path of the shock. Difference in sound speed gives rise to the development of Ritchmyer-Meshkov instabilities, converting shock energy into kinetic energy of particles and subsequently to heat.

1.4.3 Sound damping

Weak shocks generated repeatedly can be described as a superposition of sound waves. Heating by dissipation of sound then involves their frequency and also viscosity and thermal conductivity of the environment, which both scale with temperature. This dependence is, however, also influenced by the presence of magnetic field, which would decrease contribution of the thermal conductivity, as is discussed in McNamara and Nulsen (2007) and Fabian et al. (2005).

1.5 Observations

Well resolved measurements of Chandra X-ray Observatory and XMM-Newton give direct observational evidence of discussed features revealing AGN activity. Jones et al. (2007) claim that $\sim$30 % early-type galaxies also showing nuclear emission have detectable products of AGN outbursts. More recently, Shin et al. (2016) have found cavities in $\sim$52 % of systems in their sample consisting of individual galaxies, groups and clusters with extended X-ray emission observed by Chandra telescope. They also conclude that AGN activity is periodical and development of cavities is independent of environment into which they expand. This statement is in agreement with findings of Jones et al., who report disturbances in X-ray galactic haloes for both radio active (with observable radio lobes) galaxies and those with only weak nuclear emission. The spatially resolved radio signal originating in lobes extending from the very centre of galaxies is caused by synchrotron emission of relativistic electrons accelerated in the close vicinity of the central SMBH. Age of the cavities ranges from 10^6 to 10^8 yr suggesting repeating outbursts each injecting $\sim 10^{56}$ erg into the surrounding environment (Jones et al., 2007).

Global morphology of the X-ray galactic atmospheres does not always coincide with that in optical band, in other words, gravitational potential cannot be precisely estimated from X-ray isophotes. This is believed to imply that the hot gas is not in precise hydrostatic equilibrium (Diehl and Statler, 2007). Measure of discrepancy between the morphologies, on the other hand, does correlate with central X-ray and radio luminosities, which would be expectable if the AGN could be accounted for setting the motion of the gas on and redistributing it around the galaxy.

When it comes to temperature profiles, there is no general behaviour in early-type galaxies. Statler and Diehl (2007) present systems in which the temperature is outwardly rising, which is what the classical cooling flow causes in principle, are observed as well as temperature decrease with radius, implying ongoing centrally dominant heating processes (such as heating by supernovae).

Systems with temperature first outwardly rising and then falling again further out are also present among observations. What has been confirmed regarding this inconsistent behaviour is that the temperature gradients close to the centres of galaxies are strongly correlated with AGN luminosity: systems with outwardly rising temperature have high luminosity AGN and are morphologically disturbed, whereas those with negative gradients reside less luminous AGNs and seem to have less variable morphologies. Statler and Diehl also find cooling times of all atmospheres regardless discussed gradients less than a Hubble time, thus requiring a heating mechanism. This could be provided by repeating cycles of AGN activity, that would be able to create all types of observed temperature profiles.

This AGN feedback, which seems to prevent galactic atmospheres from cooling down and forming stars, can be observed in massive early-type galaxies out to numerous galaxy clusters, but is still not quite understood. Best (2007) shows that the probability that a galaxy is a radio source steepens with its mass, but there is no correlation between actual radio-luminosity of central AGN and the mass of the galaxy.

1.6 Spectral features

Spectra of the hot intergalactic gas have several characteristic components, as can be guessed from their properties mentioned in previous sections of this chapter. The gas has considerably low density (usually covered by range of $10^{-1} - 10^{-5}\,\mathrm{cm}^{-3}$) and is therefore optically thin to its own radiation. This causes the physical processes leading to the formation of its characteristic spectrum to be limited to those that involve collisions or close fly-bys of present particles. As another result of the low density, any excitation is followed by radiative de-excitation due to low collision rate.

For completeness, it should be mentioned that temperatures are in the context of high energy astrophysics often expressed in terms of energy in electronvolts using relation $E\,[\mathrm{eV}] = (k_\mathrm{B}/e)T\,[\mathrm{K}]$. This simple conversion makes temperature of 10^7 K approximately equivalent to energy of 1 keV.

1.6.1 Continuum emission

As stated in sec. 1.3, major source of X-ray emission is provided by optically thin thermal bremsstrahlung, originating from motion of charged particles in the Coulomb field. More specifically, the radiation results from the free-free interaction of electrons and protons and heavier atomic nuclei. Emissivity of bremsstrahlung is described by relation

$$\epsilon_\nu^{\mathrm{ff}} = \frac{32 Z^2 e^6 n_\mathrm{e} n_\mathrm{i}}{3 m_\mathrm{e} c^3} \sqrt{\frac{2\pi}{3 k_\mathrm{B} T m_\mathrm{e}}}\, \mathrm{e}^{-\frac{h\nu}{k_\mathrm{B}T}}\, g_{\mathrm{ff}}(T,\nu) \tag{1.9}$$

(Schneider, pg. 294), where Z is charge of ions, e denotes elementary charge, n_e and n_i number densities of electrons and ions, respectively, and m_e in denominators stand for the electron mass. Gaunt factor g_{ff} is of order 1, as estimated from approximative relation

$$g_{\mathrm{ff}} \approx \frac{3}{\sqrt{\pi}} \ln\left(\frac{9 k_\mathrm{B} T}{4 h\nu}\right).$$

From equation (1.9), the shape of the continuum component can be seen directly. For $h\nu \ll k_\mathrm{B}T$, the exponential term is negligible and the part of the spectrum is flat, whereas from $h\nu \gtrsim k_\mathrm{B}T$ the whole term is decreasing exponentially.

Another process that contributes to the continuum emission of intergalactic medium is free-bound radiation. Interpretation of the process is rather intuitive, but what should be mentioned is that the radiative recombination can dominate the spectrum at high energy tail. This applies especially to relatively low-temperature X-ray gas – compared to the extreme conditions of the intracluster medium – which can be present in massive galaxies and even cooler environments (Böhringer and Werner, 2010).

The remaining process that gives rise to the continuum spectrum of low-density plasmas is radiative transition from 2s to 1s state. In general, emission of a single photon at a given frequency is forbidden due to the conservation of angular momentum, so the de-excitation would happen through collisional excitation to higher energy state followed by permitted transition to 1s state in a sufficiently dense environment. However, in conditions of intergalactic gas, where collisions are infrequent, transition between these two states is observed and can only be ascribed to two-photon emission, which only requires the overall radiated energy to be equal to the difference of the initial and final energy level $\Delta E = E_0$. Spectrum of two-photon emission is symmetric around $E_0/2$ and spans from $E = 0$ to $E = E_0$. (Spitzer and Greenstein, 1951; Tucker and Koren, 1971; Raymond and Smith, 1977; Bottorff et al., 2006)

1.6.2 Line emission

Generally, the higher the temperature, the less prominent the line emission is. This is given by ionisation temperatures of present elements. An extreme example of a commonly observed line in rich galaxy clusters, in which the gas reaches temperatures of $1-10\,\mathrm{keV}$, is a Lyman-α line of 25-fold ionised iron, strongest just below $\sim 7\,\mathrm{keV}$. In the case of colder systems, which is usual for individual massive galaxies or groups, lines of highly ionised lighter elements can pop from the continuum emission, more specifically those with even atomic numbers (Schneider, pg. 244). Apart from dependence on temperature, the strength of individual spectral lines is sensitive also to the abundance of that particular element and obviously the density of the gas. In fig. 1.1 taken from Sanders et al. (2008), the fraction of ions in a certain ionisation state is plotted as a function of temperature of the gas, revealing information about which lines are likely to be found in spectrum of a hot galactic atmosphere.

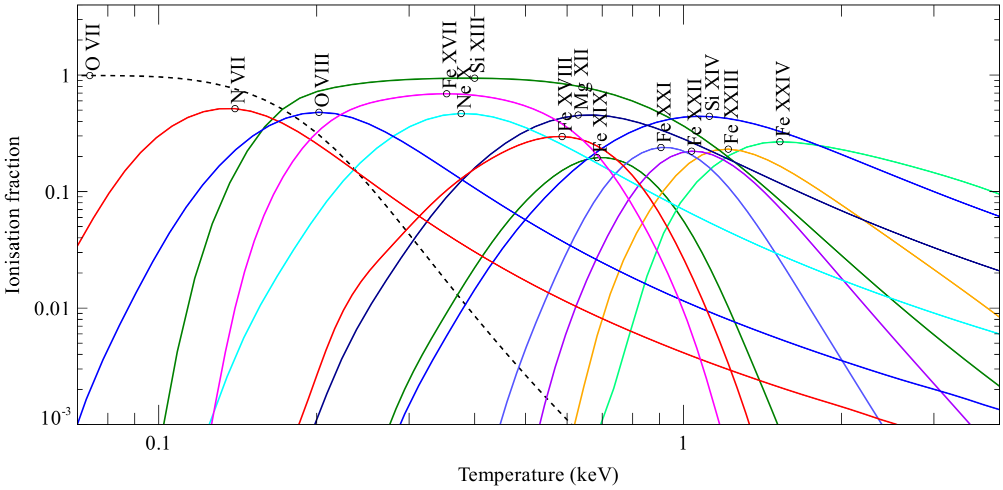

Figure 1.1: Fraction of elements in a particular ionisation state as a function of temperature in keV. Taken from Sanders et al. (2008).

1.6.3 Low-mass X-ray binaries

In addition to radiation emitted by the hot gas, an X-ray spectrum of a galaxy is enhanced by emission originating in low-mass X-ray binaries (LMXBs). These systems are composed of a primary accreting component, such as a neutron star or a black hole, and a secondary star filling up its Roche lobe from which the material flows onto a primary object.

In elliptical and S0 galaxies, LMXBs create an exclusive type of point sources of strong X-ray radiation, as others are tied to recent or ongoing star formation and which will not be discussed here with respect to the nature of the studied galaxy. At large distances, identification of the point-like origin of this radiation is beyond the resolution limit of the telescopes. Overall contribution to the galaxy spectrum has power law shape with the power-law index of about $\Gamma \sim 1.6$ as discussed in f.e. Irwin et al. (2003).

Spectral properties of this undesired component allow modelling its significance in the data independently on the gas emission. This is provided by extension of LMXBs photon energies up to 10 keV, where the radiation from the hot gas is not present, and therefore forms a sole source of radiation at high energy tail.

Chapter 2

Galaxy NGC 7049

The object studied in this work is galaxy NGC 7049 – an early-type galaxy of the southern hemisphere (Indian), which is the brightest member of a small group of six members along with NGC 7041 and NGC 7029 (Garcia, 1993).

Its morphological classification is $SA0^0$ (de Vaucouleurs et al., 1991), thus it is an unbarred lenticular galaxy of intermediate subtype – typically possessing bright bulge and disk component, usually present in spiral galaxies. Lenticulars are expected to have evolutional aspects (see Moran et al. (2007) for further details) more similar to ellipticals – their numbers decrease with increasing redshift just as of elliptical galaxies, which points to their formation in merger events or an internal process with serious effect on their structure and the star formation, which is generally much lower compared to spiral galaxies, but still more significant than in ellipticals.

Rotationally supported disk enables estimation of the distance using Tully-Fisher relation. However, a more reliable measurement has been done based on surface brightness fluctuations explained in Blakeslee (2012), positioning NGC 7049 relatively close – only 29.9 Mpc from us (Tonry et al., 2001).

This distance is still quite convenient for reliable measurements in all spectral bands. Radio emission with $L_{\mathrm{radio}} = 8.4 \times 10^{37}\,\mathrm{erg/s}$ suggests the presence of radio-mode AGN activity. Hubble image of central region (see Figure 2.1) reveals large dusty ring, scattered with blue light of young bright stars (Carlqvist, 2013), in accordance with low but non-zero star formation rate (SFR in Table 2.1).

Werner et al. (2014) present measurements of emission in Hα+[N II], a trace of warm ionised gas, and [C II] emission of cold ($\sim 100\,\mathrm{K}$) atomic gas, both extending to $r \sim 2 - 3\,\mathrm{kpc}$. More importantly, velocity distribution calculated from the [C II] line indicates that the cold gas rotates; and it seems to be formed of clumps and sheets rather than filling the space homogeneously given its low density.

The properties of the object relevant to this study are listed in Table 2.1 and are taken from mentioned paper of Werner et al. (2014).

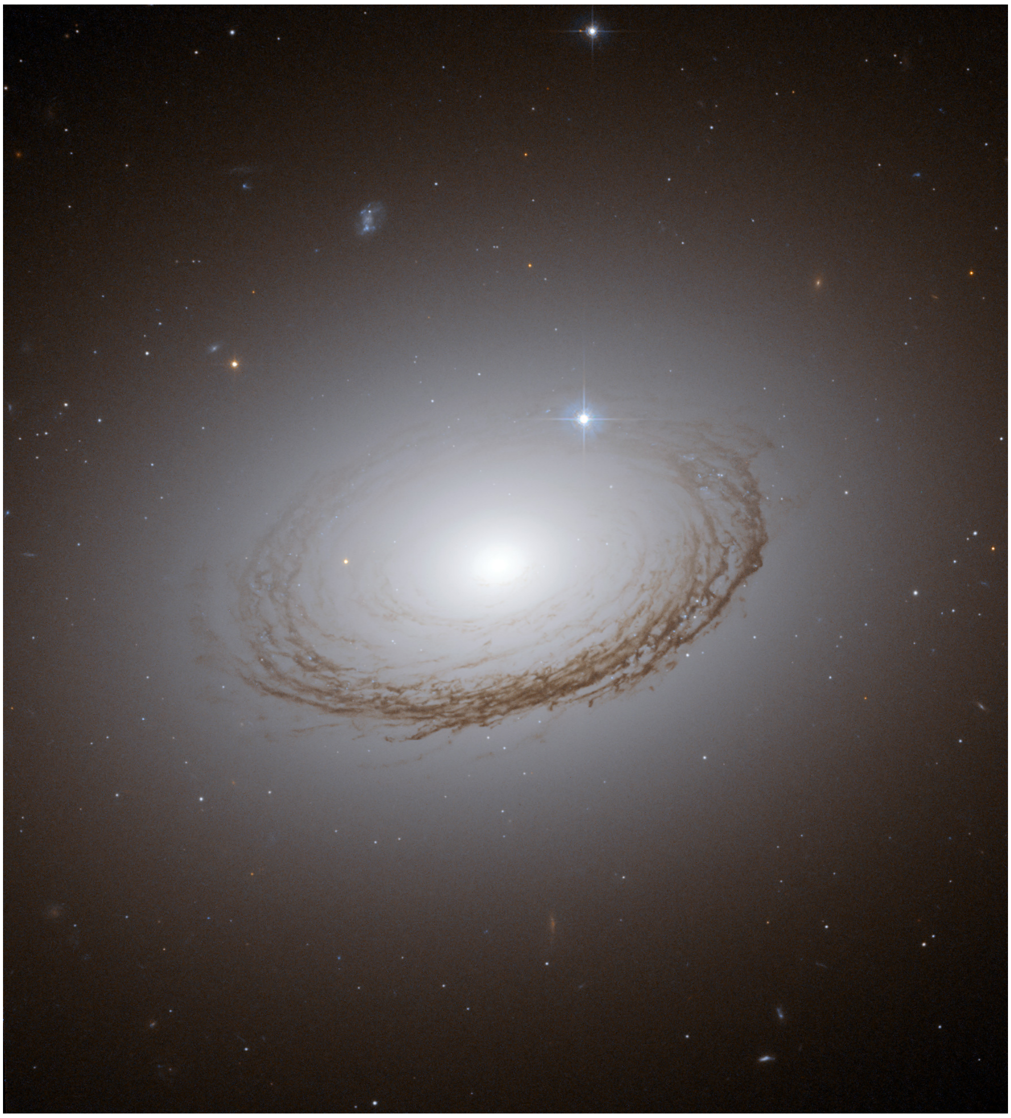

Figure 2.1: HST image of central parts of NGC 7049. Apart from the prominent dusty disk, bright bulge and flattened ellipsoidal shape of the stellar distribution is apparent.

d Mpc	z 10^{-3}	L_X 10^{41} erg/s	L_{radio} 10^{38} erg/s	$L_{H\alpha+[N\,II]}$ 10^{39} erg/s	SFR $M_\odot$/yr
29.9	7.315	1.23	0.84	31.8	0.177

Table 2.1: Properties of NGC 7049, adopted form Werner et al. (2014).

Chapter 3

Data acquisition and analysis

3.1 XMM-Newton

X-ray Multi-Mirror Mission (XMM-Newton) is an X-ray observatory of European Space Agency, which was launched in December of 1999. Being on a highly eccentric orbit with perigee of 7 000 km and apogee of 114 000 km, the lowest part is contained within the radiation belts, which limits the observations to altitudes above 60 000 km due to the high background (Jansen et al., 2001).

On board, there are three X-ray telescopes with 58 nested Walter I mirrors, each in coaxial and confocal configuration equipped with baffles preventing most of the stray light from reaching the detectors, and Optical Monitor, a Ritchey-Chrètien telescope providing simultaneous observations in the optical and ultraviolet band. The field of view is $30'$ in case of all three X-ray telescopes and the detection of the collected signal is provided by 5 instruments: 3 CCD detectors in European Photon Imaging Camera (EPIC) designed for simultaneous intensity imaging and moderate resolution spectroscopy and 2 reflecting grating spectrometers (RSG) for high-resolution spectroscopy. Since EPIC CCDs are sensitive also to the longer wavelengths (from UV down to IR), each telescope is equipped with a set of three filters. (Jansen et al., 2001; ESA, 2015)

Since only the data from EPIC camera are used in this work, the remaining instruments are left without further description.

3.1.1 EPIC-pn

EPIC-pn camera is divided into four quadrants each consisting of 3 chips (200×64 pixels) operating in parallel. All 64 channels span over a range of energies from 0.1 to 15 keV and the full width at half maximum (FWHM) of the point spread function (PSF) is in fact 12.5 arcsec. Half of the integrated energy is contained within 16.6 arcsec. In order to provide reliable spectroscopic measurements along with precise imaging, the CCDs must be operated with respect to the need of fulfilling a condition that an X-ray photon hits the detector without overlap in position and time of another photon during the integration period. The readout cycle of all 768 channels of the detector is parallel and takes 73.3 ms in the full-frame mode, in which the data for this work were acquired, from which

68.7 ms is the integration time and the rest takes the readout itself. (Strüder et al., 2001; ESA, 2015)

3.1.2 EPIC-MOS

The remaining EPIC instruments, EPIC-MOS cameras, process only 44 % of the light gathered by the telescopes, since the remaining photons are collected by RSG spectrometers. Each MOS camera consists of 7 CCDs, the central one lying exactly in the focal point of optical axis, whereas the remaining six are positioned 4.5 mm towards the mirrors in order to mimic the curvature of the focal plane. The FWHM of the PSF is in this case only ~ 4.5 arcsec, but half energy width remains similar to EPIC-pn. The readout cycle is 2.6 s, slightly increasing the risk of pile up for bright X-ray sources. Gaps around the central CCD overlap exactly for MOS cameras and are positioned at 45 degrees to the PN CCDs, providing data from a complete field of view when combined. (Turner et al., 2001; ESA, 2015)

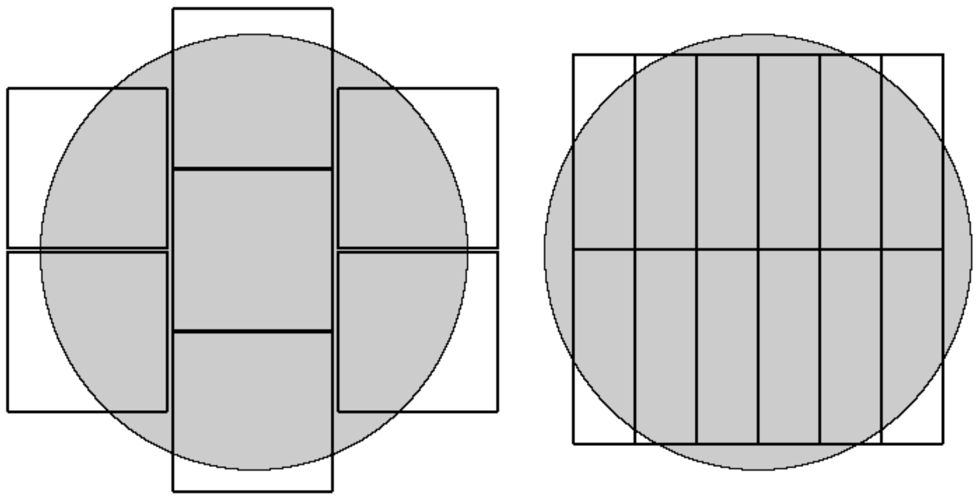

Figure 3.1: Comparison of focal plane organisation of EPIC MOS (left) and pn (right) cameras. Circles (field of view) have 30 arcmin in diameter, each of 7 EPIC MOS CCDs covers 10.9×10.9 arcmin, 12 EPIC pn CCDs occupy 13.6×4.4 arcmin each. (Taken from XMM-Newton Users Handbook (ESA, 2015), adapted.)

3.2 Background

XMM-Newton EPIC observations unavoidably contain events not related to the source, either having an instrumental or cosmic origin. Proper understanding of these background components is a challenging task especially in case of extended sources and is crucial for proper analysis of the data.

This section is therefore dedicated to inform the reader about the properties of the background components and a way of its handling in this case.

3.2.1 X-ray background

Part of the observed background are genuine X-ray photons, whose measured energy distribution is given by properties of the astrophysical source and possible presence of an absorbing medium. Here, such sources are described.

Solar wind charge exchange

Highly ionised particles escaping vicinity of the Sun as a solar wind may collide with neutral interplanetary gas or the uppermost layers of Earth's exosphere and give rise to soft X-ray photons. This process is generally referred to as the Solar wind charge exchange (SWCX) and is presented as a de-excitation of electrons in solar-wind ions, which transited from neutral particles during their encounter. It is time-variable on a timescale of days, which is considerably less compared to the variability of solar wind flux. It is especially detectable at transition lines C VI, O VII, O VIII, Ne IX, and M XI and probably even more massive particles. (Snowden et al., 2004; Carter and Sembay, 2008)

Local Hot Bubble

The Sun is located in a region with excess of an ionised matter at a temperature equivalent to 0.096 keV, the so-called Local Hot Bubble. Its thermal emission is relatively unabsorbed and the radiation emanates from distances of hundreds parsecs all over the sky. This background component does not show spatial (over the field of view) nor time variability. (Galeazzi et al., 2007)

Galactic thermal emission

Looking further out from the Sun, the Galaxy as a whole is also a source of diffuse X-ray radiation. Contrary to the Local Hot Bubble, its X-rays originally emitted by a 0.197 keV gas associated with Galactic halo are absorbed. This component is not time variable, however it is spatially dependent. (Galeazzi et al., 2007)

Unresolved point sources

Extragalactic source of undesired X-ray radiation can be attributed to faint AGNs at large distances (Hasinger et al. (1998) for example). Their emission cannot be resolved to individual sources and therefore creates diffuse and naturally spatially dependent X-ray component. Shape of the spectrum of unresolved point sources is characterised by power law with power-law index $\Gamma \approx 1.41$ (De Luca and Molendi, 2004). Given that the spectrum is relatively flat, it becomes particularly dominant at high energies ($> 5\,\mathrm{keV}$). This component is also time-independent.

3.2.2 Non-X-ray background

Apart from X-ray photons, other particles at high energies that cross the path of the telescope can either be focused by XMM-Newton's mirror shells, or simply pass through the instruments and leave traces of their encounter with the detector planes that are undistinguishable from X-ray signal.

Soft Protons component

As the spacecraft operates at relatively low altitudes (see sec. 3.1), the detectors are relatively often exposed to protons with energies comparable to soft X-rays, which are trapped in Earth's magnetosphere. These so-called soft protons (SP) are prevalent around orbit perigee but may occur any time during the observation as they are extremely unpredictable[1]. Their contribution is of two types and requires specific handling.

SP flares affect typically 30 % to 40 % of observation time and cause the spectra to be dominated by this component. These can only be eliminated by excluding the time intervals when count rate exceeds value typical for the observation. Quiescent SP contamination shows a complex spectral profile variable in both intensity and shape and is discussed in in further detail in Carter and Read (2007).

Instrumental background

When high-energy particles hit the CCDs, they can either directly produce signal (flat continuum), or initiate instrumental fluorescence. The latter is best observable in lines Al-K at $\sim 1.5\,\mathrm{keV}$ (MOS and pn), Si-K at $\sim 1.7\,\mathrm{keV}$ (MOS), less prominent contribution is from other elements present in electronic components. This component varies with time due to its origin and is also spatially variable, which is a result of inhomogeneous distribution of electronics behind the CCDs. (Carter and Read, 2007)

At energies below $0.3\,\mathrm{keV}$, electronic noise becomes obvious. Bright pixels extend into bright columns due to detector read-out and the sensitivity of the CCDs decreases. Usually, the lowest energies are excluded from any analysis.

3.3 Extraction of the spectra

For the study of NGC 7049, archival data from 3 April 2015 with observation ID 0743930101 were retrieved. Standard processing done on the data set was performed, that is constituted of the following steps.

[1]At the lowest passage, the observations are not being performed and all the instruments are closed to prevent damage to the detectors (ESA, 2015).

Raw data need to be rerun in a SAS pipeline for the event files to be created. Each event – a hit of a photon, is described by its position on a chip, arrival time and energy. From such tables, either intensity images or spectra can be gathered, filtering unwanted events. For data processing in this work, a collection of tasks developed for XMM-Newton observatory called Science Analysis System (SAS) version 15.0.0 was used as well as XMM-Newton Extended Source Analysis Software (XMM-ESAS), the one developed particularly for analysis of diffuse X-ray emission by Snowden and Kuntz (2011).

To account for the SP flaring in the data, a histogram of count rate from the field of view for each detector was generated. Usual observation shows a normal distribution and a high count rate tail. Times flagged as containing high noise due to flares (and excluded from further analysis by task *espfilt*) were having a count rate exceeding $1.5\,\sigma$ below and above peak of the Gaussian fit.

During EPIC-pn relatively long read-out time (see 3.1.1), arriving photons are assigned wrong position in the sky. Such so-called out-of-time events also need to be removed. According to the count rate at each position on the pn-chips, a model was created to mimic out-of-time events and was subsequently subtracted from the data set.

Selection of regions for extraction of spectra and removal of resolved point sources was done based on a visual inspection and with respect to the instrumental PSF. The position of the AGN ($\alpha = 21^{\mathrm{h}}19^{\mathrm{m}}0.17^{\mathrm{s}}$, $\delta = -48^{\circ}33''43.45'$) was determined from an observation done by Chandra X-ray Observatory, which disposes of much better spatial resolution – only 0.5 arcsec. To exclude most of the point-source emission, they were encircled with radius 10 arcsec. For an inspection of the galactic emission properties, the region in which the brightness could be attributed to the hot gas was divided into six concentric annuli with the largest reaching to 165 arcsec, (approximately 21.7 kpc) from the centre. Additionally, one more annulus was added with inner radius equal to the outer of the sixth annulus and its outer border much further out from the galaxy (255 arcsec or 28.3 kpc). These were then divided into four quadrants, for which the orientation was chosen with respect to the rotational axis of the galaxy.

Events geometrically belonging to the selected region and satisfying other conditions recommended for a reliable analysis were then added to the file of an OGIP format. Such files typically contain a table of the number of counts per energy bin, integration time and information concerning f.e. background scaling factors. Apart from the spectra themselves, any spectral analysis software requires two additional files – an Ancillary Response File (ARF) and a Redistribution Matrix File (RMF), which describe the response of the particular detector. ARFs contain combined effective area of the telescope, filter and the detector multiplied with the quantum efficiency as a function of energy. Applying ARF to the input spectra creates a distribution of counts observed with perfect energy resolution. To account for this imperfection, RMF is used. They store a 2-D matrix of probabilities at which a photon of a certain wavelength is assigned to a given energy channel. For high-resolution instruments, this matrix would be nearly diagonal.

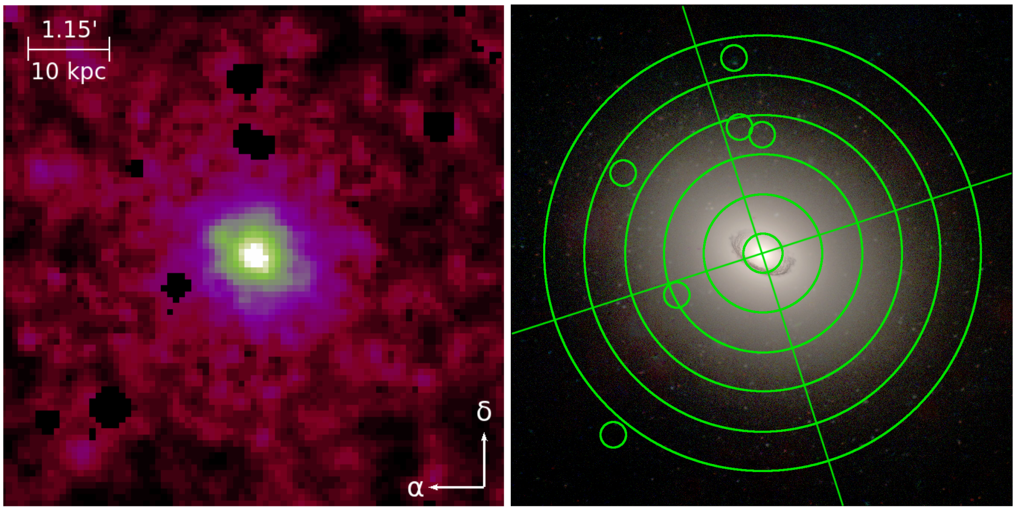

(a) (b)

Figure 3.2: X-ray image of NGC 7049 (a) and the optical counterpart (b) from Carnegie-Irvine Galaxy Survey, combined with Hubble image of the central region and overlaid with lines visualising regions for extraction of the spectra. Small circles label point sources, which were cut out from the X-ray image and spectral analysis. Distance of adjacent circles is 30″, that is twice the instrumental PSF. In the XMM-Newton image is a composition of data from all EPIC instruments, exposure-corrected and adaptively smoothed. The images are identically oriented but not in scale.

3.4 Spectral Analysis

For most of the fitting, the well-maintained software package SPEctral X-ray and UV modelling and analysis (Kaastra et al., 1996), abbreviated as SPEX, was used. This software provides various models well describing properties of radiation in short wavelengths and multiple fitting methods that allow the user to handle the data as needed. In the following section, models and the fitting process used in this work are shortly described.

3.4.1 Models

When developing an accurate model for a spectrum of the galactic emission, some information about processes which influenced the photons on their path to the detector need to be known prior to fitting. These generally are the distance to the galaxy and the column density of absorbing particles in between of the telescope and the source of radiation.

Each model for the galaxy was constructed of several additive components, which have a parameter determining the flux, and a multiplicative part that operates on the additive models. Those utilised in this case are listed below.

cie – A collisional ionisation equilibrium (CIE) additive model whose parameters are among others normalisation, temperature and elemental abundances. Even its original purpose was to model a single temperature plasma, it can be used as a differential emission measure model where the emission measure as a function of $k_{\mathrm{B}}T$ has a Gaussian shape (usually denoted as GDEM) with additional parameter `sig`. In that case, the code evaluates number of isothermal *cie*s with the temperature parameter set as the mean temperature T and `sig` being the width σ_T of the Gaussian profile of emissivity

$$Y(T) = \frac{1}{\sqrt{2\pi}\sigma_T} \frac{Y_0}{e^{-(T-T_0)^2/2\sigma_T^2}}. \tag{3.1}$$

We remind that the differential emission measure is defined in eq. (1.2). The GDEM multitemperature variant of *cie* model is denoted as *gdem* further on.

cf – An additive model for an isobaric cooling flow described by equation (1.7). The cooling function $\Lambda(T)$ is evaluated for half-solar abundances by default.

pow – Power law additive model with basic parameters being the normalisation A and a photon index Γ, which defines the steepness of the photon flux decrease as a function of energy $F(E) = AE^{-\Gamma}$.

reds – This multiplicative model applies the effect of the redshift to selected additive components associated with the source at a distance described by redshift z.

hot – A collisional ionisation equilibrium multiplicative model for absorption by particles present at a certain temperature and column density. Counter-intuitively, this model also allows to mimic an environment of a low temperature, which is present in the Galaxy and was used here for this purpose.

3.4.2 Fitting method

A method developed for parameter estimation of a model fit on data sets typical for X-ray astrophysics, that is low count rates per a large number of bins, is the C-statistic introduced by Cash (1979). Suppose that $\{X_i, i \in [1, N]\}$ are the realisations (the data) of a model described by parameters Θ drawn from some distribution. Expected values M_i can be predicted from the model for each data point and are used in definition of the likelihood function

$$\mathcal{L}(X_i) = \mathrm{Prob}(X_1, X_2, ...X_N|\Theta) = \prod^{N} \mathrm{Prob}(X_i|M_i(\Theta)), \tag{3.2}$$

in which the $\text{Prob}(X_i|M_i(\Theta))$ is the probability of the ith data point having value X_i while the predicted value M_i for the model with parameters Θ.

This is a foundation for the C, which is defined for data with Poission distribution

$$\mathcal{P}(n;\mu t) = \frac{e^{-\mu t}(\mu t)^n}{n!}. \tag{3.3}$$

In case of spectral data, the $\mathcal{P}(n;\mu t)$ is the probability that n photons (X_i) over the exposure time t are received, while μ is the average count rate ($M_i(\Theta)/t$ of the ith energy bin). Our likelihood function is then

$$\mathcal{L}(X_i) = \prod^{N} \mathcal{P}(X_i|M_i(\Theta)) \tag{3.4}$$

where

$$M_i = t \int \text{RMF}(i, E) \cdot \text{ARF}(E) \cdot \mathcal{M}(E) \cdot \text{d}E. \tag{3.5}$$

$\mathcal{M}$ stands here for the physical model and is multiplied by the detector response. The C statistic itself is defined with use of natural logarithm of the likelihood function in which the $X_i!$ is omitted for it is model independent.

$$C = -2 \ln \mathcal{L} = 2 \sum_i (M_i - X_i \ln M_i) \tag{3.6}$$

The reasoning behind choosing C-statistic instead of commonly known χ^2 is that it does not assume prior knowledge of the Gaussian variation of the data or that they are Gaussian at all. That implies an important benefit that it does not require any binning of the data[2], which are typically sparse (and follow Poisson distribution). Such a step ultimately leads to the loss of information and is undesirable in X-ray astrophysics, in which every photon counts.

The fitting was done on data lying in energy bins of $0.3 - 5.0\,\text{keV}$. Even the X-ray emission of NGC 7049 is soft, dominating at energies below $2\,\text{keV}$, the remaining counts at higher energies are crucial for the successful and reliable analysis. The power law spectrum of LMXBs is shallow and dominates at harder energies. Its normalisation is therefore primarily constrained based on the $2 - 5\,\text{keV}$ energy band. Additionally, the data at energies of $1.38 - 1.60\,\text{keV}$ were not fitted due to residual contamination with instrumental lines. Since binning in X-ray astrophysics should be used with extreme caution and only where its application is well justified, we did the analysis using unbinned data with no exception.

The multiplicative components of any model here had all the required parameters known. One of them is particle column density of the absorbing medium,

[2]Unless the background subtraction leads to a negative number of counts per bin, which was not the case here.

for which was here used the value[3] of $N_{\mathrm{HI}} = 2.70 \times 10^{20}\,\mathrm{cm}^{-3}$ provided by Leiden/Argentine/Bonn Survey (Kalberla et al., 2005) and the redshift $z = 0.007315$ (Paturel et al., 2002). Throughout the analysis, solar abundances of Lodders et al. (2009) and Hubble parameter $h_0 = 0.73$ were used.

Since the spectra are inevitably influenced by projection effects, under the assumption of spherical symmetry the deprojection analysis was done. With Xspec fitting package (Arnaud, 1996) and its model *projct*, the spectra were fitted simultaneously and so any contribution of the outer shells to the emission originating below it was taken into account.

All results in the following chapters are presented with 1σ error and error bars on x-axes of all plots stand for the spans of the annuli. For handling the results from spectral analysis, we took advantage of Python programming capabilities (van Rossum, 1995) and its specialised libraries Scipy (Jones et al., 2001–), Numpy (Dubois et al., 1996) and Matplotlib (Hunter, 2007).

[3]It could seem more reasonable to include molecular hydrogen to computations (which would, in this case, add about 10 %). It has been proven, however, that N_{HI} gives more reliable results and thus is recommended (Prof. Dr. Jelle S. Kaastra, private communication).

Chapter 4

Results

4.1 X-ray surface brightness

The X-ray image of NGC 7049 (Figure 3.2a) reveals geometric properties of the highly-energetic emission regardless its origin. With information of orientation of the disk, it can be seen that the shape only slightly deviates from radial symmetry. More pronounced this deviation is at smaller radii, corresponding to the position of the stellar disk. If this feature mimics the distribution of the hot gas, thanks to the annular shape of the regions selected for extraction of the spectra, an enhancement in density would occur in apparently brighter sectors. A reasonable assumption of axial symmetry would require this departure to be observable in both sides of the plane of the stellar disk. As described below, no such enhancement was detected and assumption of spherical symmetry of the gaseous component is appropriate.

The *cie* normalisation in SPEX is proportional to the density squared times volume of the emitting region (or more precisely, to $n_{\mathrm{H}}n_{\mathrm{e}}V$). Having this value for four quadrants at six distances from the centre from spectral fits, we were able to constrain the projected particle density of the plasma. The results are written in Table 4.1 and displayed in Figure 4.1. Excluding the contribution of LMXBs, the profiles reflect only the gas density. As can be seen in Figure 4.1, there is no significant departure from radial symmetry. Clearly, the LMXB component follows the distribution of stars, that may differ from the diffuse plasma significantly and thus alter appearance of X-ray brightness of the galaxy.

A characteristic proposed early after first observations of diffuse X-ray emission from massive galaxies and clusters is a specific shape of the surface brightness profile. A simple model proposed by Cavaliere and Fusco-Femiano (1976), based on isothermality of the self-gravitating sphere of plasma permeating these systems, has been in an enhanced version (Cavaliere and Fusco-Femiano, 1978) used ever since. The β-model proposes the gas particle density n to decrease with radius as

$$n(r) = n(0)\left[1 + \left(\frac{r}{r_{\mathrm{c}}}\right)^2\right]^{-3\beta/2}, \tag{4.1}$$

where r_{c} is the core radius and β being a function of velocity dispersion σ and temperature (both spatially invariant) as $\beta = \mu m_{\mathrm{H}}\sigma/k_{\mathrm{B}}T$. We fitted the deprojected particle density profile with this model with β, $n(0)$ and r_c free parameters yielding $\beta = 0.41 \pm 0.02$. The model is plotted along with the data in Figure 4.4.

As the conditions required by the model are generally not satisfied, relevance of this result may be questionable. However, as Arnaud (2009) claims in his commentary to the original paper, even perhaps more accurate analytical models are presented nowadays, the β-model should not be abandoned for being inappropriate either from observational or theoretical side. It has proven itself successful in fitting the data with only a few free parameters and gives a reasonable estimate of basic characteristics in a first approximation, when its limitations are taken into account.

R_{in} [$''$]	R_{out} [$''$]	n_{A} [$10^{-3}\mathrm{m}^{-3}$]	n_{B} [$10^{-3}\mathrm{m}^{-3}$]	n_{C} [$10^{-3}\mathrm{m}^{-3}$]	n_{D} [$10^{-3}\mathrm{m}^{-3}$]
0	15	$132.7^{+8.4}_{-7.7}$	$117.9^{+8.2}_{-8.0}$	$99.4^{+9.6}_{-8.9}$	$132.4^{+8.0}_{-7.6}$
15	45	$13.4^{+1.4}_{-0.5}$	$21.2^{+3.4}_{-3.7}$	$17.0^{+3.5}_{-2.3}$	$22.6^{+9.7}_{-10.2}$
45	75	$5.4^{+1.6}_{-1.2}$	$7.3^{+1.5}_{-1.5}$	$8.3^{+1.8}_{-1.6}$	$7.4^{+2.1}_{-1.8}$
75	105	$2.5^{+0.3}_{-0.4}$	$2.8^{+0.3}_{-0.3}$	$2.8^{+0.3}_{-0.3}$	$3.1^{+0.2}_{-0.2}$
105	135	$1.7^{+0.2}_{-0.2}$	$2.0^{+0.2}_{-0.2}$	$1.8^{+0.2}_{-0.2}$	$1.9^{+0.2}_{-0.2}$
135	165	$1.4^{+0.1}_{-0.1}$	$1.5^{+0.2}_{-0.2}$	$1.5^{+0.1}_{-0.1}$	$1.5^{+0.2}_{-0.2}$

Table 4.1: Particle densities in all four sectors from projected spectra. Subscripts determine direction, in which the density was measured. A and C lie in rotational axis, whereas B and D lie perpendicular to it.

4.2 Global features

Here we present properties of the galaxy as a whole derived from its spectrum. For this purpose, we used an annular region spanning from $15''$ to $165''$ from the galaxy centre. The innermost region was excluded due to contamination by AGN power-law shaped spectrum with an unknown photon index.

The isothermal CIE model did not sufficiently cover galactic emission, therefore we derived the results listed below from the fit with a model $\mathcal{M}_{\mathrm{g}}$ containing Gaussian differential emission model to describe the X-ray emitting gas. More specifically, the model had the form of that in equation (4.2) and the final fit of the spectrum can be found in Figure 4.2.

$$\mathcal{M}_{\mathrm{g}} = \mathit{hot} \times \mathit{reds} \times (\mathit{gdem} + \mathit{pow}). \tag{4.2}$$

There are more possibilities how to cover spectrum of multitemperature plasma in collisional ionisation equilibrium. Commonly used are two *cie* components at different temperatures, usually the second being by a factor of 1/2 or

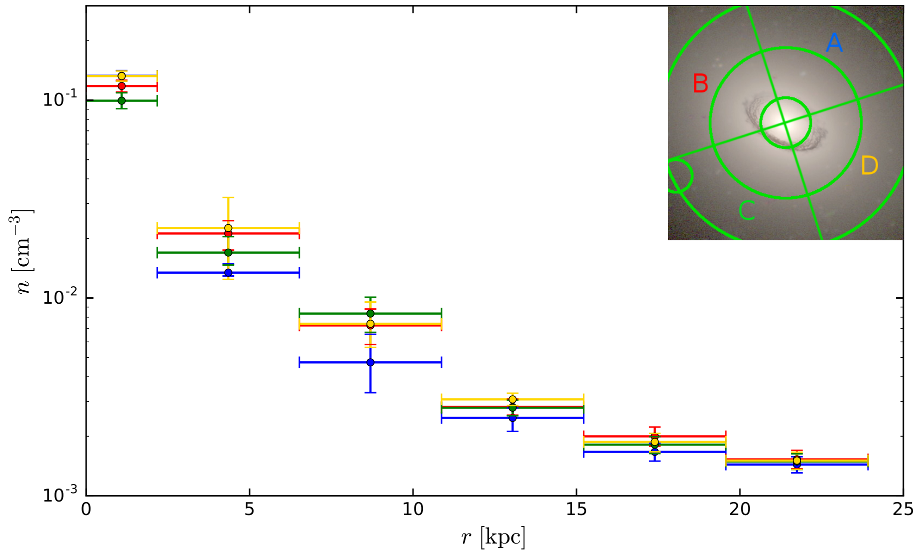

Figure 4.1: Particle densities measured in four directions: blue and green in direction parallel to rotational axis of the cold gas disk and red and yellow perpendicular to it. For clarity, the disk and orientation is shown in small image in upper right.

3/4 lower than the first and then fitted while tied together. Such model would of course describe a plasma at exactly two distinct temperatures, which is poorly physically motivated.

GDEM is the most natural choice for fitting a non-isothermal spectrum, adding only one free parameter to the model, which is a highly desirable property when dealing with low signal spectra.

Photon index of the power-law component accounting for bulk X-ray properties of LMXBs in NGC 7049 was set to the value of $\Gamma = 1.6$ according to findings of Irwin et al. (2003) with only the normalisation left as a free parameter. In this case, reasonably high quality of the data allowed us to constrain the overall metallicity. The abundances were tied for elements usually observable at temperatures expected for this source, i.e. O, Ne, Mg, Si, S, Ar, Ca, Fe, Ni and scaled together. Abundance of the remaining metals was set to value of 0.5 solar and fixed. With this approach, we found the emission weighted temperature of the gas to be $k_{\mathrm{B}}T = 0.43^{+0.02}_{-0.01}$ keV and emission weighted metallicity of $Z = 0.7^{+0.2}_{-0.1}\,Z_{\odot}$.

4.3 Radial profiles

As the surface brightness profiles show remarkable similarity with no significant deviations in any direction, the choice of circular-shaped regions for spectral

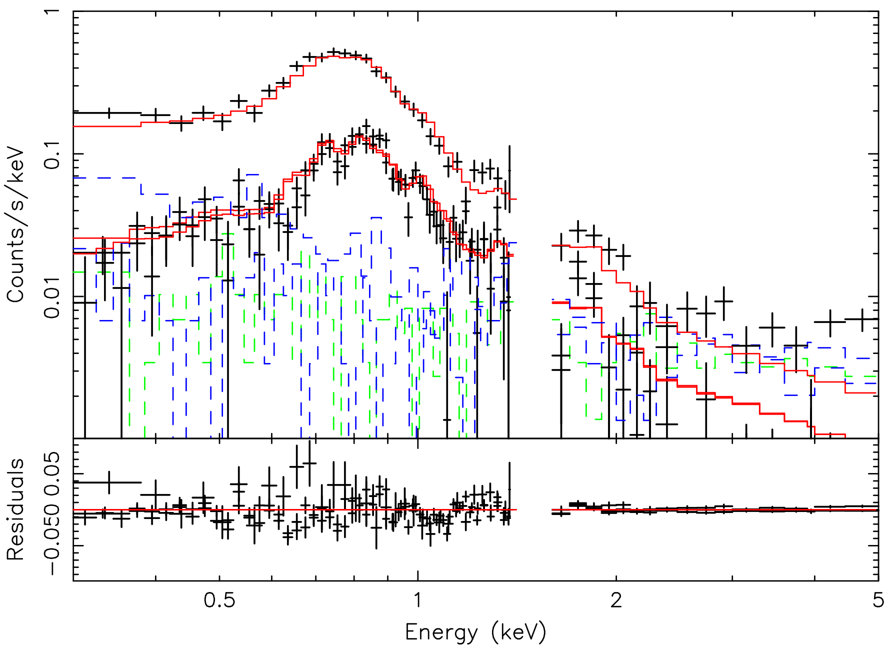

Figure 4.2: Spectrum of NGC 7049. Local background subtracted data (black) (binned automatically using *obin*, Kaastra and Bleeker (2016), and manually at high energy tail only for plotting purposes) are fitted with model $\mathcal{M}_{\rm g}$ (red colour, see (4.2) for the description). The contribution of the background to the data is shown in blue and green dashed lines. The three sets of the data and models are for MOS1, MOS2 (lower) and pn (upper) detector.

analysis has proven itself justified. As the central region is necessarily contaminated with AGN emission, the power-law emission should be of two kinds here – the LMXBs component with known $\Gamma = 1.6$ and the AGN with $\Gamma_{\rm AGN}$ free. However, one power-law component with free photon index described the two sources sufficiently well, with $\Gamma_{\rm AGN+LMXB} \approx 1.73$.

We fixed the $\Gamma_{\rm AGN+LMXB}$ at this value for the deprojection analysis, using single temperature CIE model *vapec* for the hot gas and *wabs* for the absorption in Xspec. A common problem that appears when fitting this kind of spectra is anticorrelation of metallicity and normalisation.

This is caused by relatively low energy resolution of the instruments and nature of the plasma. Individual emission lines merge together forming wide bumps raising above continuum. Therefore, based on the global fit and inability to constrain the metallicity with high accuracy, we fixed it to 0.5 Solar as is commonly done in these situations. Leaving both normalisation and metallicity free leads to unphysical results of the fit, as it was also in this case.

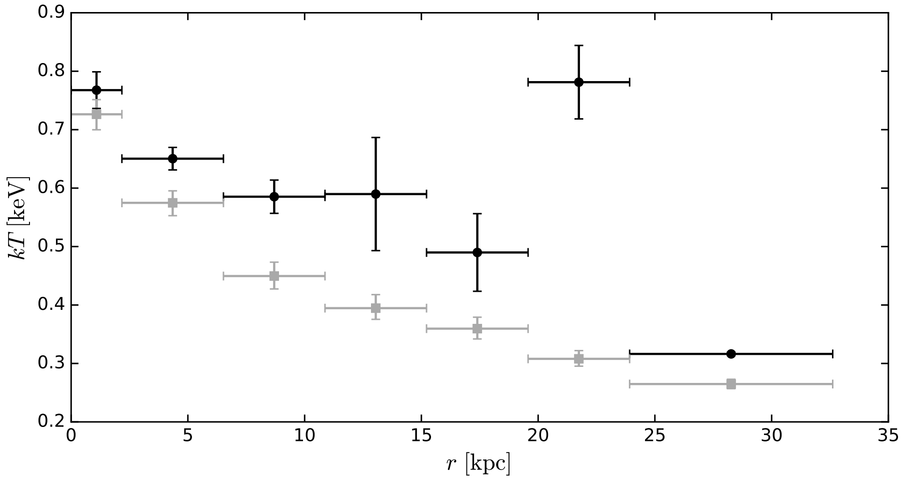

Figure 4.3: Temperature radial profile of the galaxy derived from deprojected (black circles) and projected spectra (grey squares). The jump at 22 kpc is likely an artefact of the spectral deprojection.

In Figure 4.3 we present the temperature profile for all seven annuli, the results obtained from the deprojected spectra in black circles, while values determined from projected spectra as grey squares for comparison. The fact that the global negative temperature gradient is broken in the sixth annulus is likely to be an artefact induced by simultaneous fitting of all data sets. This feature is a common result of relatively weak emission attributed to a component with free parameters being subjected to deprojection and was described in Russell et al. (2008). As can be seen in the plot, analysis of projected spectra in SPEX did not show any increase in temperature.

In Table 4.2, temperature and normalisation (norm) of deprojected spectra are listed, where units of normalisation are standard Xspec units, from which the electron number density can be derived knowing angular diameter distance D_A and redshift z of the source and volume of a particular shell V_shell from relation

$$n_\mathrm{e} = 10^7(1+z)D_\mathrm{A}\sqrt{\frac{4\pi\,\mathrm{norm}}{V_\mathrm{shell}\,n_\mathrm{e}/n_\mathrm{H}}} \approx 157\sqrt{\frac{\mathrm{norm}}{R_\mathrm{out}^3 - R_\mathrm{in}^3}}, \tag{4.3}$$

in which norm is in cm^{-3} and R_in and R_out are the respective outer and inner radii of the shell in arcsec.

From the temperature and the best-fit normalisation, the particle number density, entropy, and pressure were calculated. The entropy K used here is different from entropy in statistical physics and is defined simply as

$$K = k_\mathrm{B}Tn_\mathrm{e}^{-2/3}, \tag{4.4}$$

$R_{\rm in}$ [″]	$R_{\rm out}$ [″]	$k_{\rm B}T$ [keV]	norm [10^{-5} cm^{-3}]
0	15	0.77 ± 0.03	2.9 ± 0.2
15	45	0.65 ± 0.02	7.6 ± 0.3
45	75	0.59 ± 0.03	6.7 ± 0.3
75	105	0.60 ± 0.10	4.1 ± 0.3
105	135	0.49 ± 0.07	4.3 ± 0.6
135	165	0.78 ± 0.06	3.3 ± 0.5
165	225	0.316 ± 0.003	30.7 ± 0.7

Table 4.2: Results from deprojected spectra extracted from seven annuli centred with respect to the position of the AGN. For the outermost annulus, only the temperature is relevant, since the normalisation is enhanced with emission from all the gas above the outer radius of the shell. The units for normalisation are standard Xspec units described by eq. (4.3).

where $n_{\rm e}$ is electron number density and k is Boltzmann constant. This definition makes our entropy proportional to statistical specific entropy and thus retains its meaning, avoiding calculation of natural logarithm. Simply said, the high entropy gas floats, whilst low entropy causes the gas to sink.

For determination of the pressure p we used relation

$$p = nk_{\rm B}T, \tag{4.5}$$

reminding that n is total particle number density calculated as $n = 1.92\, n_{\rm e}$. The profiles are shown in Figure 4.4. Note that the last data point is not presented in any of the figures and is excluded from all calculations, as to the normalisation, the contribution of all layers of gas lying above the seventh shell contribute to its gas density due to projection effect and the value is therefore artificially enhanced.

The green line in $n(r)$ stands for the β-model discussed in section 4.1 and blue dashed line in the bottom panel displaying $p(r)$ is fit of an empirical pressure model (here denoted as p-model) with the form of

$$p(r) = \frac{p(0)}{\left(\frac{r}{a}\right)^b + \left(\frac{r}{a}\right)^c}, \tag{4.6}$$

where $p(0)$, a, b and c are free parameters. This model is a simplification of the 'universal' model for galaxy clusters introduced by Arnaud et al. (2010) and is used only in order to estimate its gradient used further on. Unfortunately, the parameters were strongly correlated and poorly constrained, thus unsuitable for use.

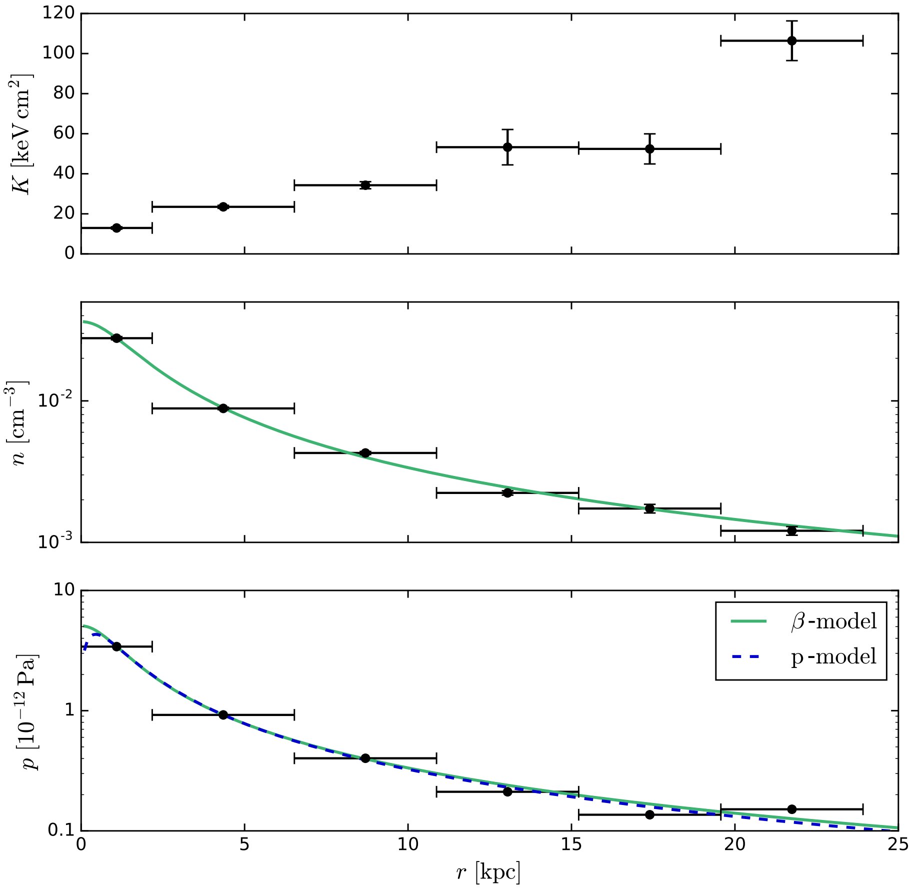

Figure 4.4: Profile of entropy $K = k_\mathrm{B} T n_\mathrm{e}^{-2/3}$, particle density n and pressure $p = n k_\mathrm{B} T$. Green curves are in both cases β-models ((4.1) and (4.7)) fitted to the data and the blue dashed curve stands for the pressure profile defined in eq. (4.6). We note that errors especially in the bottom plot are too small to be visible.

We therefore fitted the pressure profile with β-model in form analogous to the one in (4.1), that is

$$p(r) = p(0) \left[1 + \left(\frac{r}{r_\mathrm{c}'} \right)^2 \right]^{-3\beta'/2}, \tag{4.7}$$

achieving remarkable accordance with results from the p-model. As the β-model was fitted with significantly better precision, we used it for our calculations below.

4.4 Profiles in sectors

Subdividing the emission allowed us to create profiles of the hot gas emission in plane of rotation and the direction perpendicular to the disk. At this place, we remind that the inclination of the plane of rotation is $i \approx 30°$. The values obtained for the temperature and normalisation from the deprojection are all written in Table 4.3 for sectors in rotational axis, named A and C in accordance with the notation shown in the Figure 4.1, and Table 4.4 for sectors in plane of rotation, denoted as B and D. Again, they are listed for all seven distances from the galaxy centre, with only the temperature being reliably fitted at the last one. The results are displayed in figures 4.5 and 4.6, where the data for sectors A+C are plotted in blue-green and for sectors B+D orange is used, again for consistency with choice of colours in Figure 4.1.

Temperature profile in Figure 4.5 shows clear departures at ~ 22 kpc, again most probably accountable to the complicated fitting process as in case of temperature profile assuming spherical symmetry of the problem in previous section, rather than real physical jumps in properties of the hot plasma.

Results for gas density confirm our previous findings about spherical symmetry of the gas, obvious from remarkable similarity of the gas distribution in both directions.

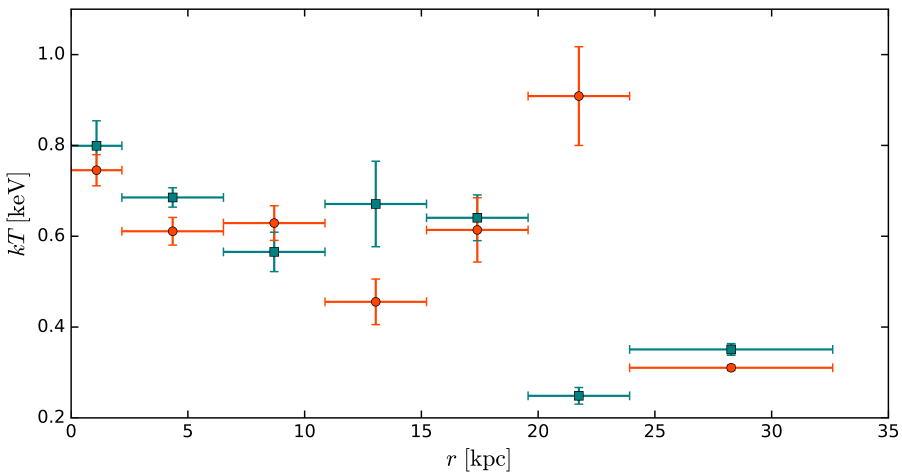

Figure 4.5: Temperature profile for sectors in rotational axis and direction perpendicular to it showed in blue-green and orange, respectively.

4.5 Cooling process

Rotating cold molecular gas appearing as a thin disc that spans over a very few kiloparsecs in the galactic centre, most prominent in an image captured by Hubble Space Telescope in Figure 2.1 may indicate an ongoing cooling of the

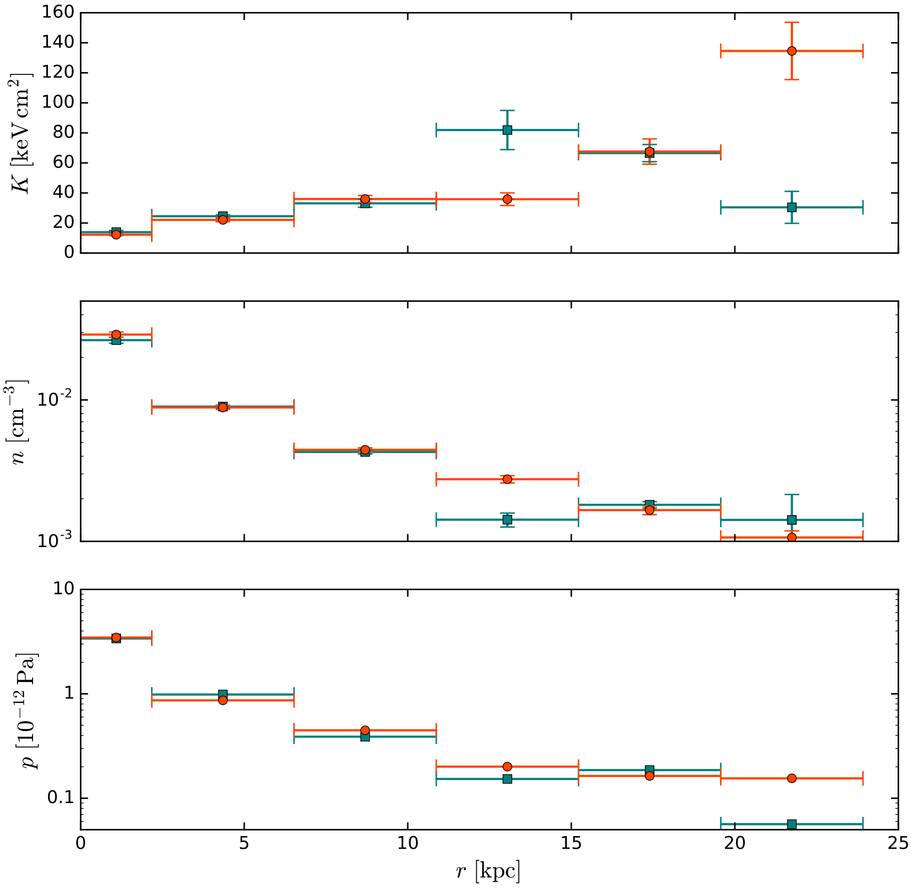

Figure 4.6: Profile of entropy $K = k_\mathrm{B} T n_\mathrm{e}^{-2/3}$, particle density n and pressure $p = n k_\mathrm{B} T$ in sectors parallel with rotational axis (blue-green) and perpendicular direction (orange). We note that errors especially in the bottom plot are too small to be visible.

$R_{\mathrm{in}}\,['']$	$R_{\mathrm{out}}\,['']$	$k_{\mathrm{B}}T$ [keV]	norm $[10^{-5}\,\mathrm{cm}^{-3}]$
0	15	0.80 ± 0.06	0.65 ± 0.06
15	45	0.69 ± 0.02	1.95 ± 0.09
45	75	0.57 ± 0.04	1.7 ± 0.1
75	105	0.67 ± 0.09	0.41 ± 0.09
105	135	0.64 ± 0.05	1.2 ± 0.1
135	165	0.25 ± 0.02	1.1 ± 1.2
165	225	0.35 ± 0.01	7.2 ± 0.2

Table 4.3: Values of temperature and normalisation obtained from deprojected spectral fits to the data in sectors lying in rotational axis of the galaxy (A and C).

$R_{\mathrm{in}}\,['']$	$R_{\mathrm{out}}\,['']$	$k_{\mathrm{B}}T$ [keV]	norm $[10^{-5}\,\mathrm{cm}^{-3}]$
0	15	0.75 ± 0.03	0.78 ± 0.07
15	45	0.61 ± 0.03	1.9 ± 0.1
45	75	0.63 ± 0.04	1.8 ± 0.1
75	105	0.46 ± 0.05	1.5 ± 0.2
105	135	0.61 ± 0.07	1.0 ± 0.1
135	165	0.91 ± 0.11	0.6 ± 0.1
165	225	0.31 ± 0.01	8.4 ± 0.3

Table 4.4: Values of temperature and normalisation obtained from deprojected spectral fits to the data in sectors lying in plane of rotation (B and D).

X-ray gas onto a non-radial orbit in the plane of rotation. To test whether such process is present and detectable by means of X-ray spectroscopy, we searched for multitemperature gas in both directions.

As the gas emission is proportional to density squared, it is expected to form clumps of cooling matter at different temperatures, giving rise to a more complicated spectrum. This is then better described by a differential emission measure distribution in general simply broader than a delta function, which is on the contrary the case of a single temperature CIE model. For this purpose, we used the model described in (4.2), that has GDEM for our target component, in SPEX, and analysed properties of gas in sectors once again.

We measured non-zero σ_T with more than 99.73 % significance in the B+D sector of the second annulus ($15''-45''$, which corresponds to $4.3-8.7$ kpc, denoted as $(\mathrm{B}+\mathrm{D})_{(2)}$ further on), whilst in the perpendicular direction, $(\mathrm{A}+\mathrm{C})_{(2)}$, no such feature was observed. More precisely, we measured $\sigma_{T,\mathrm{B+D}} = 0.21^{+0.05}_{-0.06}$ keV with mean temperature $k_{\mathrm{B}}T_{\mathrm{B+D}} = 0.51^{+0.03}_{-0.03}$ keV in $(\mathrm{B}+\mathrm{D})_{(2)}$ and $\sigma_{T,\mathrm{A+C}} = 0.00^{+0.07}_{-0.00}$ keV in region $(\mathrm{A}+\mathrm{C})_{(2)}$. Implicitly, the range of temperatures in the plasma of $(\mathrm{B}+\mathrm{D})_{(2)}$ is approximately $(0.30; 0.72)$ keV.

Under the assumption that it is the radiative cooling that triggers the presence of a multitemperature plasma, we can put constraints on the cooling rate. We therefore fitted an isobaric cooling flow model (assuming the plasma is not supported by a magnetic field) cf onto the spectrum of $(\mathrm{B}+\mathrm{D})_{(2)}$ constructed as

$$\mathcal{M}_{\mathrm{cf}} = \mathit{hot} \times \mathit{reds} \times (\mathit{cf} + \mathit{pow}), \tag{4.8}$$

resulting in mass deposition rate $\dot{M} \sim 10^{-2}\, M_{\odot}/\mathrm{yr}$. More accurate estimate could not be made since the cooling function in eq. (1.7), which describes the isobaric cooling flow, is strongly dependent on abundance of heavier elements, which cannot be properly measured in this case. The mass deposition rate was estimated with $Z = 0.7\, Z_{\odot}$, abundances measured from the global spectrum and are used in calculations further on, for it is possible that the metallicity would be closer to this value and it also makes further results more conservative.

Simulations from recent years (Sharma et al., 2012) show that thermal instabilities can only develop in the hot medium of galaxies, groups, and clusters if the ratio of cooling time and free-fall time is less than ten. Observations of clusters seem to confirm this relation, f.e. those presented by McCourt et al. (2012), and so should be the case of NGC 7049.

We calculated the free-fall time simply as

$$t_{\mathrm{ff}} = \sqrt{\frac{2r}{g}}, \tag{4.9}$$

where gravitational acceleration g is derived from the pressure profile introduced in eq. (4.6) as

$$g = -\frac{1}{\rho}\frac{\mathrm{d}p}{\mathrm{d}r} = -\frac{1}{n m_{\mathrm{H}} \mu}\frac{\mathrm{d}p}{\mathrm{d}r}. \tag{4.10}$$

The cooling time, described in eq. (1.3), was calculated with the cooling function for abundance received from the global fit in sec. 4.2. The results for t_{ff}, t_{cool} and their ratio are all listed in tables 4.5 and 4.6 and displayed in Figure 4.7. Apparently, the criterion for development of multiphase gas observed in this galaxy does not hold. The discrepancy does not originate in the X-ray measurement, as Sharma et al. (2012) suggests that the inequality $t_{\mathrm{cool}}/t_{\mathrm{ff}} \lesssim 10$ should also indicate the presence of H_{α} emission. This has been well confirmed in NGC 7049.

To test thermal stability of the hot gas, we calculated also the Field stability parameter (Field, 1965), which was used for similar purpose in paper of Werner et al. (2014) and is defined as

$$\Pi_{\mathrm{F}} = \frac{\kappa T}{n_{\mathrm{e}} n_{\mathrm{H}} \Lambda(T) r^2}, \tag{4.11}$$

where κ is thermal conductivity and $\Lambda(T)$ is the cooling function. It can be interpreted as a measure of prevalence of conductive heating rate over the radiative cooling rate on scales close to r. The limiting value for Π_{F} based on a sample of

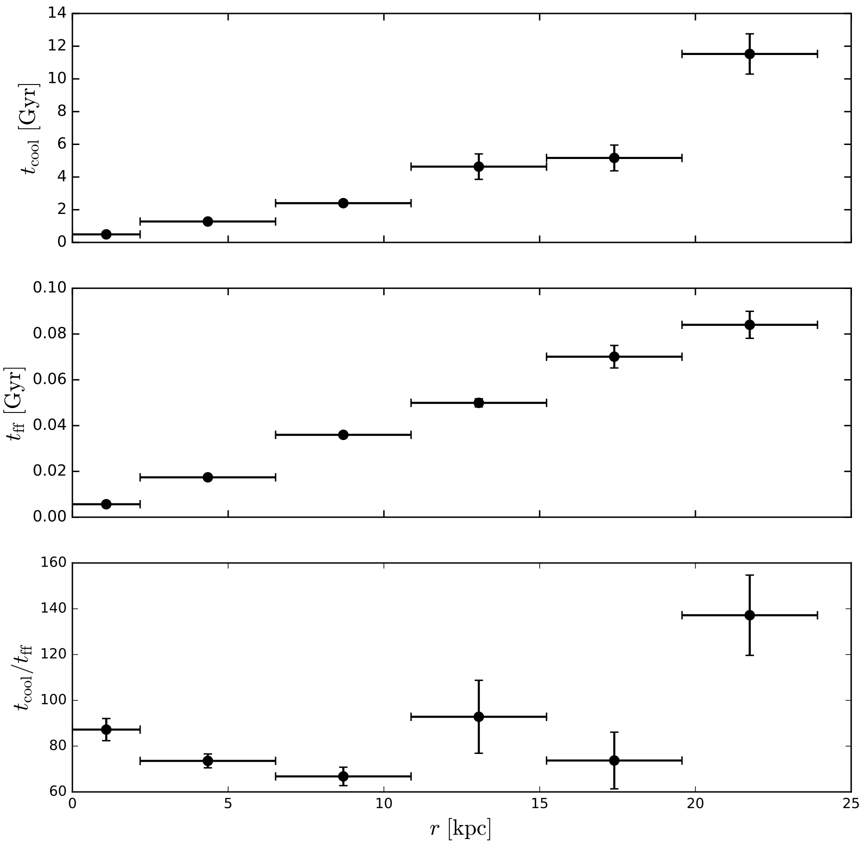

Figure 4.7: Profiles of cooling time, free-fall time and their ratio evaluated for the six distances from central AGN. According to Sharma et al. (2012), only if the ratio $t_{\rm cool}/t_{\rm ff}$ falls below 10, thermal instabilities can form in the X-ray gas.

46 brightest galaxies of their cluster examined in Voit et al. (2008), under which the thermal conduction is not capable of suppressing radiative cooling, is $\Pi_{\rm F} \lesssim 5$.

As can be seen in Figure 4.8, where the observationally suggested threshold is visualised through the red line, the condition is not (fully) met again. Even though our data suggest presence of multi-phase gas surrounding disk of the cold, the critical value of Field stability criterion is still lower. However, this result is somewhat comparable to a similar case; elliptical galaxy NGC 6868, also revealing presence of *rotating* disk of cold gas (Werner et al., 2014) surrounded by extended halo of hot plasma, is also rather comparable to systems without traces of low-temperature gas. Werner et al. expect such behaviour conditioned by rotational (or other) support in their work.

A parameter that should be more robust in rotating systems in determining the conditions required for thermal instabilities to develop takes into account viscosity of the possibly cooling medium. It is defined as

$$\Pi_\nu = \frac{\nu t_{\rm cool}}{r^2} \tag{4.12}$$

with ν being kinematic viscosity of the gas and $t_{\rm cool}$ and r cooling time and distance to the galaxy centre, respectively, as usual. It introduces the viscous diffusion length in a cooling time (square root of the nominator in (4.12)) and compares it to r. According to (Werner et al., 2014), instabilities can develop only if $\Pi_\nu \lesssim 1$. The parameters $\Pi_{\rm F}$ and Π_ν are not completely independent, as the processes they are based on are both due to Coulomb collisions of either electrons or ions. Their ratio is $\Pi_\nu/\Pi_{\rm F} \simeq 0.0253$, yielding $\Pi_\nu \lesssim 0.13$. Results from calculation of the viscosity parameter are presented in Figure 4.8, where the red line symbolises the critical value and indeed show similar results. For calculation of the last two stability criteria, we used the code of Dr. Paul Nulsen. As the code does not return errors, for they are generally not presented in literature in such cases and their proper calculation is not trivial, we estimated them by varying input values by their error and choosing the maximal to have a robust guess of errors. These are also included in Table 4.6.

$R_{\rm in}$ [″]	$R_{\rm out}$ [″]	$t_{\rm cool}$ [Gyr]	$t_{\rm ff}$ [Gyr]
0	15	0.49 ± 0.02	0.0057 ± 0.0002
15	45	1.28 ± 0.05	0.0174 ± 0.0004
45	75	2.4 ± 0.1	0.0360 ± 0.0009
75	105	4.6 ± 0.8	0.050 ± 0.002
105	135	5.2 ± 0.8	0.070 ± 0.005
135	165	11.5 ± 1.2	0.084 ± 0.006

Table 4.5: Cooling time and free-fall time calculated from values obtained in the spectral analysis of the six annuli.

$R_{\rm in}$ [″]	$R_{\rm out}$ [″]	$t_{\rm cool}/t_{\rm ff}$	$\Pi_{\rm F}$	Π_ν
0	15	87 ± 5	20 ± 4	0.53 ± 0.09
15	45	74 ± 3	7.1 ± 0.8	0.18 ± 0.02
45	75	67 ± 4	5 ± 1	0.13 ± 0.02
75	105	93 ± 16	9 ± 6	0.2 ± 0.2
105	135	74 ± 12	4 ± 2	0.11 ± 0.06
135	165	137 ± 18	28 ± 10	0.7 ± 0.3

Table 4.6: The three parameters used for determining whether thermal instabilities can develop: cooling time over free-fall time, Field parameter and viscous parameter.

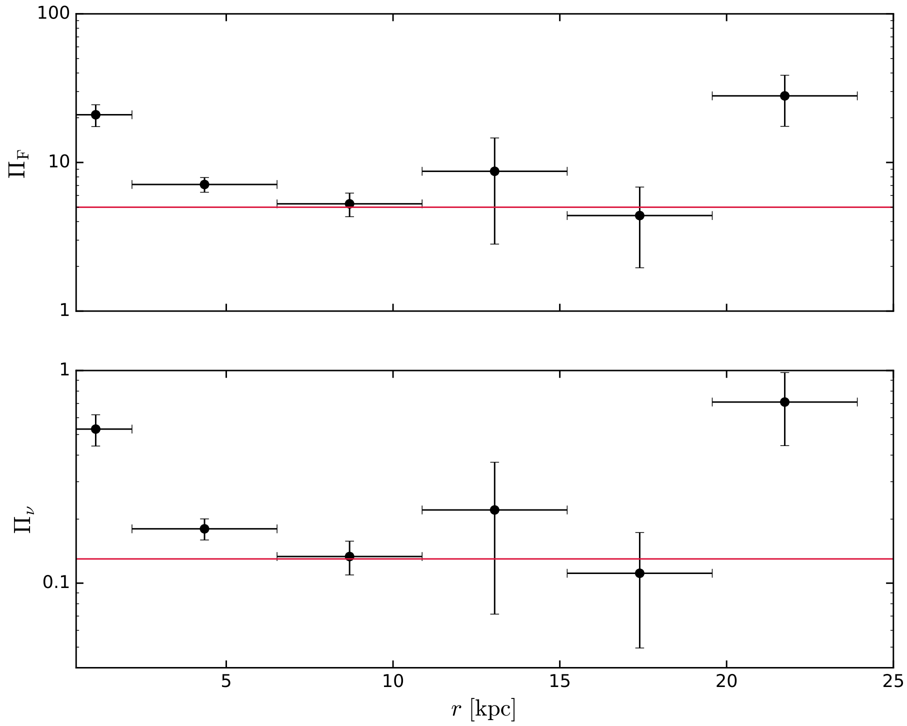

Figure 4.8: Field stability parameter (top) and viscous stability parameter (bottom) as a function of radius. The red line in upper panel expresses limit value, that should be an upper limit for thermal stability of the hot gas. In the lower panel, similar threshold is approximately equal to 0.13.

Chapter 5

Discussion

We measured physical properties of hot gas permeating fast-rotating lenticular galaxy NGC 7049, which could be read from its X-ray spectrum. Interpretation of our results and their comparison to other objects and models is a subject of this chapter.

5.1 Shape of the X-ray halo

The image of the X-ray-emitting gas (contaminated with radiation of low-mass X-ray binaries and possibly other unresolved point sources) and further on the projected spectral analysis suggests that no significant flattening is directly observable in the hot gas. However, what Brighenti and Mathews (1996, 1997) predict from numerical simulations is flattening of the plasma and formation of extensive disks of hot gas.

Since this has not been observed as commonly as expected among studied objects[1], they also provided several reasons for it. As a possible explanation of this effect being absent, they suggest that the gas is either supported by magnetic field originating in stellar mass loss, or that the system has been subjected to alteration of angular momentum resulting from a merger event in its recent history. Additionally, according to their models, sufficiently cold gas should obscure X-rays at smaller radii and therefore create an additional darkening of the X-ray emission, unless the gas forms small clumps. If the collapse of cooling gas continued to form stars, they would need to have initial mass function skewed towards low-mass stars, so that it didn't result in contradiction with unobserved massive blue stars. Furthermore, at large radii, the flattening can be effectively suppressed by galactic winds. Brighenti and Mathews (1996)

It is unlikely that the gas would be obscured to compensate for the excess of X-ray emission due to flattening. The X-ray halo spans over larger volumes and the absorption would need fine tuning to darken the X-ray gas behind so that the overlying gas would add up the exact amount of X-rays to create spherically symmetric image of the galaxy we observe.

Hanlan and Bregman (2000) studied relatively small sample of 6 nearby objects with various rotational speed and for fastest rotating galaxies found smaller X-ray

[1] By the time the paper was published, in fact no such feature had been observed.

ellipticity than what is observed in optical band. Lenticular galaxy NGC 6861 shows flattened isophotes of X-ray gas (Machacek et al., 2010), but as a member of a group is currently undergoing a merger event. Generally, observation of hot gas in rotating galaxies is more challenging due to systematically lower X-ray luminosities, due to rotationally reduced depth of gravitational potential wells, as presented in Negri et al. (2014).

5.2 Spectral properties

From global spectrum, we estimated the metallicity of the gas to be $Z = 0.7^{+0.2}_{-0.1}\,Z_{\odot}$ which is a value roughly comparable to other early-type galaxies. However, the result may be influenced by our assumption of solar composition of the gas and certainly a constant abundance over the X-ray halo. Gradients of content of metals in ellipticals is presented f. e. in Tozuka and Fukazawa (2008) and shows that constant metallicity is not common. There are also cases in which the metallicity increases with radius, but such trends are rather exceptional.

It is no surprise that variation of elemental abundances reflects history of chemical enrichment via supernovae and composition of stars contributing to the hot gas with stellar winds. Difference can therefore be relatively large for individual elements, we refer to Ji et al. (2009) as an example. Unfortunately, there is no reliable method to constrain the abundances for spectra like ours, with low number of counts.

Overall, the difference in metallicity measured and the real one results in biased normalisation. For sane shifts from $Z = 0.5\,Z_{\odot}$ used in the analysis of spatially distinguished spectra – suppose metallicity underestimated or overestimated by a factor of 2, would result in density being overestimated or underestimated by 25 %, respectively. Accordingly, the pressure would be influenced by the same factor and the entropy would be affected even less – it would be smaller or larger by 17 % respectively. Gradients in metallicity would also slightly alter the slopes of models fitted to them.

Emission weighted temperature measured here with GDEM model is among early-type galaxies (excluding brightest cluster galaxies) not outstanding and nor is the temperature profile. An example for all could be the sample of 53 elliptical galaxies with extended X-ray gas in work of Fukazawa et al. (2006). Authors did not distinguish between fast-/slow-rotators in their work, but based their criterion ($n_{\mathrm{e}}(r = 10\,\mathrm{kpc}) < 3 \times 10^{-3}\,\mathrm{cm}^{-3}$), the NGC 7049 would be among low-density objects, that possess all positive, negative, or variable temperature profiles, while galaxies of higher densities in their sample had temperatures mostly raising with distance from the centre. Concerning the temperature determined from global spectrum, a number of rotating galaxies observed with Chandra X-ray Observatory have similar X-ray temperatures Posacki et al. (2013).

We compared our entropy profile with those of galaxies in the work of Werner et al. (2014). They examined properties of galaxies with and without extended H_{α} emission, including NGC 6868, an elliptical galaxy with rotating disk of cold gas. In Figure 5.1 we plotted the entropy profile again along with data from Werner et al.

Non-rotating systems of their sample divide into two distinct profiles, while NGC 7049 and NGC 6868, both rotating early-type galaxies having extended H_α emission, tend towards higher entropy galaxies without it. Entropy profile of NGC 7049 is flatter than the one of NGC 6868 and its innermost value is relatively high. Combined with the information of negative temperature profile, we can conclude that some centrally positioned heating mechanism influenced the hot gas component. When the entropy of gas was centrally raised, pressure of surrounding medium led to increase of gas temperature and subsequently its observed radially decreasing trend.

The heating could have been provided either by AGN activity, merger, or high supernovae rate. While frequent stellar explosions would be unable to preserve the cold disk, which would need to form after the supernovae became less common, AGN outflows would not necessarily destroy it. On the other hand, if the gas of infalling galaxy was not stripped off in outskirts of NGC 7049, it could have generated the cold disk itself. The latter two scenarios are discussed in the following section in further detail.

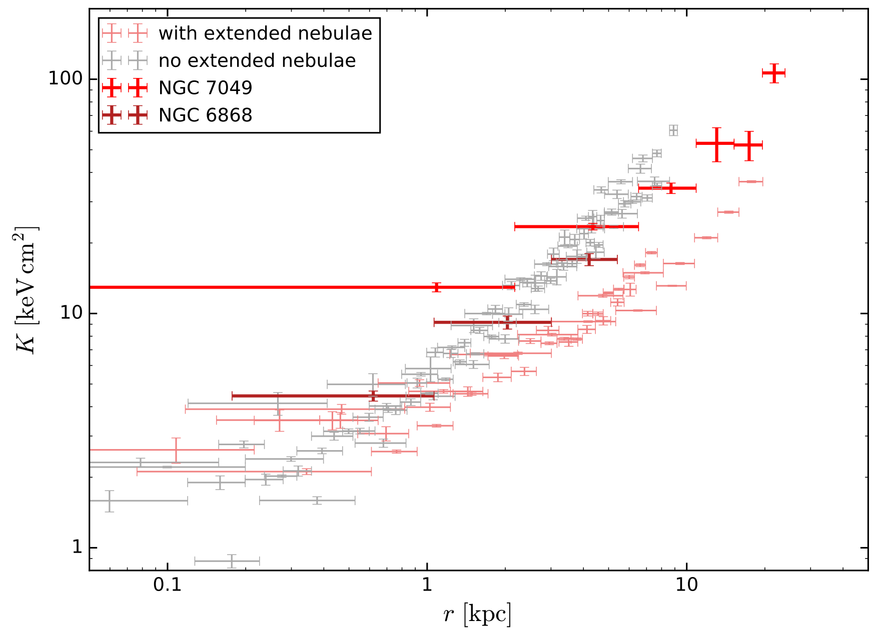

Figure 5.1: Entropy profile of sample of galaxies from Werner et al. (2014) (grey, pink and dark red) and entropy of NGC 7049. NGC 6868 also possesses extended H_α emission in form of a rotating disk. Note that the x-axis is in logarithmic scale as well.

5.3 Cooling process

At distance of 15″ to 45″ from the centre in sectors lying in the plane of rotation, we have measured with high precision a presence of multitemperature X-ray gas using differential emission measure model with Gaussian distribution of emissivity. Such feature was not detected in directions perpendicular to the rotational plane. Additionally, inner part of this region, from which was the spectrum extracted, contains cold atomic gas. These features suggest an ongoing process of cooling, but criteria which should indicate conditions needed for development of thermal instabilities give contradictory results. This either comes from inadequacy of the criteria under conditions of this system, or the gas indeed is thermally stable and the observed features are of a different origin.

The criterion introduced in Sharma et al. (2012) assumes the gas is supported exclusively by buoyancy. If the cooling is set on in the gas, its entropy locally decreases and the cooling amount of gas starts moving inwards into the medium of lower entropy. If it can reach the radius at which the entropy is the same fast enough, the cooling will stop and the flow inwards will terminate.

This is where the rotational support might be crucial. The time for the cooling clump of gas with non-zero angular momentum to move inwards is longer than in previous case, and therefore the gas can cool at its current rate. With this scenario, the criterion of $t_{\mathrm{cool}}/t_{\mathrm{ff}} \lesssim 10$ would not be strictly followed and the thermal instabilities would develop even when the ratio was larger than 10. The actual limiting value would then depend on other processes that have influence on mixing of the cooling gas with surrounding environment, dissipation of angular momentum, such as viscosity and turbulence.

Similar impact could be expected for support by magnetic field. However, a moderate magnetic field of $B \sim 10^{-10}\,\mathrm{T}$ would generate pressure $p_{\mathrm{B}} = B^2/2\mu_0 \sim 4 \times 10^{-15}\,\mathrm{Pa}$, which would be in case of central thermodynamic pressure measured in NGC 7049 of order of 10^{-4} smaller and thus its dynamical properties would be negligible.

If, however, the criteria were reliable and there indeed was no cooling in progress, then the shape of the spectrum well fitted with GDEM model would have to be created differently. The fact that the signs of multitemperature plasma were measured only in plane of rotation is in favour of this spectral property having origin in the galaxy itself. We fitted the regions on both sides of the galaxy separately to ensure that two distinct components of hot gas in opposite directions did not cause the effect. The best-fit was again obtained with GDEM, having the same temperatures from both spectra.

Stellar origin of X-rays contaminating the spectrum should also be considered. As mentioned earlier, star formation rate in NGC 7049 is low, of order of $0.1\,\mathrm{M}_{\odot}/\mathrm{yr}$, and thus we can conclude that the galaxy does not possess many bright O-B stars. Their contribution to observed X-rays is likely not to have any significance. High-mass X-ray binaries can also be excluded for they too require massive progenitors and more importantly, their emission would only result in increase of normalisation of power-law component. Obviously, not only young and massive stars are X-ray emitters, but including spatial distribution of stellar mass to these considerations, we expect this possible explanation to be of lesser importance.

If the hot gas did not form the dusty disk through developing thermal instabilities and cooling onto a non-radial orbit, it could have either condensed from stellar mass-loss, or been brought to place by merger event.

The stellar winds are commonly expected to assimilate into the hot gas of massive galaxies via thermal conduction. Voit and Donahue (2011) pointed to a scenario according to which the gas should remain relatively cool and be an important source of material for new stars. The stellar mass-loss will likely be replenished when the pressure of the surrounding hot gas is low. On the other hand, for low central entropies and high pressure, the gas might partly retain its thermal properties. In case of this galaxy, the central entropy is relatively high and pressure of the surrounding hot medium would probably not be able to prevent the star-ejected gas from being swept out. Nevertheless, perhaps the possibility of such contribution should not be completely ruled out.

Observations of NGC 7049 in H_α and N II carried out by Very Large Telescope and analysed in Coccato et al. (2007) reveal presence of an inner disk of a ionised gas orthogonal to the main sense of rotation that is a few arcsec wide. The fact that the gas in the inner polar disk is geometrically decoupled from the main one, it cannot be attributed to a single gaseous component of a strongly warped disk. As Coccato et al. claim, this feature is not rare among lenticular galaxies, but it cannot be ruled out that it has been created in an accretion of matter from an infalling galaxy. A merger event could have contributed to creation of the cold disk, a raise of central entropy and negative temperature gradient. This would, however, not exclude the possibility of ongoing cooling process and would not explain presence of the indication of a multi-temperature gas.

Regardless its origin, the presence of cold gaseous disk suggests that the AGN somehow avoids destroying it. AGN driven feedback in form of collimated outbursts propagating mainly perpendicular to the disk without dissipating in its vicinity would be capable of preserving it. Other possibility would be that the AGN has been inactive for time long enough for the disk to form. Rotational support of the gas would also alter accretion rate and feeding of the AGN.

Special attention to rotating galaxies with AGN and extended X-ray halo was paid in Gaspari et al. (2015). They modelled the AGN feedback cycle for these systems, suggesting creation of the cold disk, followed by accretion of cold gas onto the black hole. AGN-connected heating processes should then raise entropy of the gas to the level at which cooling instabilities cannot develop. During the violent heating processes triggered by AGN, the disk should be able to survive. This process would explain relatively high entropy of the hot phase and also the observed H_α-emitting disk. According to their findings, the cooling at $t_{\rm cool}/t_{\rm ff} > 10$ should certainly not lead to formation of filamentary structure of cooling gas, while the disk-like configuration is a more favourable outcome.

Chapter 6

Summary and conclusions

In this thesis, we focused on properties of X-ray halo of lenticular galaxy NGC 7049. In the first chapter, we introduced basic processes leading to the formation of the hot gas permeating massive galaxies. The classical cooling flow was explained with its possible consequences, followed by mechanisms inducing additional heating of the hot medium. Apart from the theoretical point of view, we provided short summary of observational evidence for mentioned signs of both heating and cooling. The shape of X-ray spectrum of the hot gas is described, followed by classification of all sources of background. We introduced the galaxy as an object deeply interesting for studying in X-ray bands, a massive system with non-zero angular momentum possessing a disk of atomic gas near its centre.

Then, the practical part is briefly described, firstly outlining construction of XMM-Newton satellite and instruments on board used for data acquisition. We mentioned data reduction and subsequently the spectral analysis, focusing also on description of fitting method preferable for use in X-ray astrophysics.

In Chapter 4 we presented geometrical shape of the X-ray emitting gas and its general spectral properties, concluding that any gas flattening is undetectable. From spatially resolved spectroscopy we measured generally negative gradient of temperature and, compared to other early-type galaxies, a relatively high central entropy, suggesting that a centrally positioned heating mechanism shaped the hot gas into this structure. From analysis of radial profile subdivided into two sectors – one in plane of rotation and one in direction perpendicular to it, we found nearly identical physical properties, assuming that the jumps in temperature and other quantities were caused by oscillations during deprojection with *projct*.

In region lying in plane of rotation of the second annulus, we measured multi-temperature plasma with more than 99.73 % significance, while in perpendicular direction, no such feature was observed. Multitemperature plasma suggests an ongoing process of cooling, and therefore we tested thermal stability of the hot gas based on Field stability parameter, viscous criterion and ratio of the cooling time and the free-fall time. The latter, setting threshold value for cooling to $\lesssim 10$, is not satisfied at any radius, while the Field parameter and viscous criterion are much closer to the critical value. However, the $t_{\rm cool}/t_{\rm ff}$ might not be the indicative criterion when applied to rotating galaxies. We discussed alternative explanations of observed features in the previous section.

The AGN feedback and subsequently the evolution of galaxies in different conditions are still puzzling and hotly debated topics among scientists, and perhaps an intensive and systematic search for common X-ray gas properties of fast-rotators might foreshadow answers to the ubiquitous questions surrounding these systems.

Bibliography

K. A. Arnaud. XSPEC: The First Ten Years. In G. H. Jacoby and J. Barnes, editors, *Astronomical Data Analysis Software and Systems V*, volume 101 of *Astronomical Society of the Pacific Conference Series*, page 17, 1996.

M. Arnaud. The β-model of the intracluster medium. Commentary on: Cavaliere A. and Fusco-Femiano R., 1976, A&A, 49, 137. A&A, 500:103–104, June 2009. doi: 10.1051/0004-6361/200912150.

M. Arnaud, G. W. Pratt, R. Piffaretti, H. Böhringer, J. H. Croston, and E. Pointecouteau. The universal galaxy cluster pressure profile from a representative sample of nearby systems (REXCESS) and the Y_{SZ} - M_{500} relation. A&A, 517:A92, July 2010. doi: 10.1051/0004-6361/200913416.

A. Baldi, W. Forman, C. Jones, R. Kraft, P. Nulsen, E. Churazov, L. David, and S. Giacintucci. The Unusual X-Ray Morphology of NGC 4636 Revealed by Deep Chandra Observations: Cavities and Shocks Created by Past Active Galactic Nucleus Outbursts. ApJ, 707:1034–1043, December 2009. doi: 10.1088/0004-637X/707/2/1034.

E. F. Bell, C. Wolf, K. Meisenheimer, H.-W. Rix, A. Borch, S. Dye, M. Kleinheinrich, L. Wisotzki, and D. H. McIntosh. Nearly 5000 Distant Early-Type Galaxies in COMBO-17: A Red Sequence and Its Evolution since z˜1. ApJ, 608:752–767, June 2004. doi: 10.1086/420778.

P. N. Best. Radio-loud agn heating in elliptical galaxies and clusters. In H. Böhringer, G. W. Pratt, A. Finoguenov, and P. Schuecker, editors, *Heating versus Cooling in Galaxies and Clusters of Galaxies*, pages 166–171. Springer-Verlag Berlin Heidelberg, 2007.

J. P. Blakeslee. Surface brightness fluctuations as primary and secondary distance indicators. Ap&SS, 341:179–186, September 2012. doi: 10.1007/s10509-012-0997-6.

H. Böhringer and N. Werner. X-ray spectroscopy of galaxy clusters: studying astrophysical processes in the largest celestial laboratories. A&A Rev., 18:127–196, February 2010. doi: 10.1007/s00159-009-0023-3.

Mark C. Bottorff, Gary J. Ferland, and Joseph P. Straley. Twophoton transitions and continuous emission from hydrogenic species. *Publications of the Astronomical Society of the Pacific*, 118(846):1176, 2006. URL `http://stacks.iop.org/1538-3873/118/i=846/a=1176`.

F. Brighenti and W. G. Mathews. Structure and Evolution of Interstellar Gas in Flattened, Rotating Elliptical Galaxies. ApJ, 470:747, October 1996. doi: 10.1086/177905.

F. Brighenti and W. G. Mathews. Evolution of Interstellar Gas in Rapidly Rotating Elliptical Galaxies: Formation of Disks. ApJ, 490:592–604, December 1997. doi: 10.1086/304900.

P. Carlqvist. Model of outgrowths in the spiral galaxies NGC 4921 and NGC 7049 and the origin of spiral arms. Ap&SS, 343:689–712, February 2013. doi: 10.1007/s10509-012-1270-8.

J. A. Carter and A. M. Read. The XMM-Newton EPIC background and the production of background blank sky event files. A&A, 464:1155–1166, March 2007. doi: 10.1051/0004-6361:20065882.

J. A. Carter and S. Sembay. Identifying XMM-Newton observations affected by solar wind charge exchange. Part I. A&A, 489:837–848, October 2008. doi: 10.1051/0004-6361:200809997.

W. Cash. Parameter estimation in astronomy through application of the likelihood ratio. ApJ, 228:939–947, March 1979. doi: 10.1086/156922.

A. Cavaliere and R. Fusco-Femiano. X-rays from hot plasma in clusters of galaxies. A&A, 49:137–144, May 1976.

A. Cavaliere and R. Fusco-Femiano. The Distribution of Hot Gas in Clusters of Galaxies. A&A, 70:677, November 1978.

E. Churazov, M. Brüggen, C. R. Kaiser, H. Böhringer, and W. Forman. Evolution of Buoyant Bubbles in M87. ApJ, 554:261–273, June 2001. doi: 10.1086/321357.

L. Coccato, E. M. Corsini, A. Pizzella, and F. Bertola. The search for inner polar disks with integral field spectroscopy: the case of NGC 2855 and NGC 7049. A&A, 465:777–786, April 2007. doi: 10.1051/0004-6361:20066214.

A. De Luca and S. Molendi. The 2-8 keV cosmic X-ray background spectrum as observed with XMM-Newton. A&A, 419:837–848, June 2004. doi: 10.1051/0004-6361:20034421.

G. de Vaucouleurs, A. de Vaucouleurs, H.G. Corwin, R.J. Buta, G. Paturel, and P. Fouque. *Third Reference Catalogue of Bright Galaxies (RC3)*. Springer-Verlag: New York, 1991.

S. Diehl and T. S. Statler. Morphological signatures of agn feedback in the hot interstellar medium of normal elliptical galaxies. In H. Böhringer, G. W. Pratt, A. Finoguenov, and P. Schuecker, editors, *Heating versus Cooling in Galaxies and Clusters of Galaxies*, pages 155–160. Springer-Verlag Berlin Heidelberg, 2007.

Paul F. Dubois, Konrad Hinsen, and James Hugunin. Numerical python. *Computers in Physics*, 10(3), May/June 1996.

G. Elwert. Verallgemeinerte Ionisationsformel eines Plasmas. *Zeitschrift Naturforschung Teil A*, 7:703–708, November 1952. doi: 10.1515/zna-1952-1102.

ESA. *XMM-Newton Users Handbook*, 2015. Issue 2.13 (ESA: XMM-Newton SOC).

S. M. Faber, C. N. A. Willmer, C. Wolf, D. C. Koo, B. J. Weiner, J. A. Newman, M. Im, A. L. Coil, C. Conroy, M. C. Cooper, M. Davis, D. P. Finkbeiner, B. F. Gerke, K. Gebhardt, E. J. Groth, P. Guhathakurta, J. Harker, N. Kaiser, S. Kassin, M. Kleinheinrich, N. P. Konidaris, R. G. Kron, L. Lin, G. Luppino, D. S. Madgwick, K. Meisenheimer, K. G. Noeske, A. C. Phillips, V. L. Sarajedini, R. P. Schiavon, L. Simard, A. S. Szalay, N. P. Vogt, and R. Yan. Galaxy Luminosity Functions to z˜1 from DEEP2 and COMBO-17: Implications for Red Galaxy Formation. ApJ, 665:265–294, August 2007. doi: 10.1086/519294.

A. C. Fabian, C. S. Reynolds, G. B. Taylor, and R. J. H. Dunn. On viscosity, conduction and sound waves in the intracluster medium. MNRAS, 363:891–896, November 2005. doi: 10.1111/j.1365-2966.2005.09484.x.

G. B. Field. Thermal Instability. ApJ, 142:531, August 1965. doi: 10.1086/148317.

W. Forman, P. Nulsen, S. Heinz, F. Owen, J. Eilek, A. Vikhlinin, M. Markevitch, R. Kraft, E. Churazov, and C. Jones. Reflections of Active Galactic Nucleus Outbursts in the Gaseous Atmosphere of M87. ApJ, 635:894–906, December 2005. doi: 10.1086/429746.

Y. Fukazawa, J. G. Botoya-Nonesa, J. Pu, A. Ohto, and N. Kawano. Scaling Mass Profiles around Elliptical Galaxies Observed with Chandra and XMM-Newton. ApJ, 636:698–711, January 2006. doi: 10.1086/498081.

M. Galeazzi, A. Gupta, K. Covey, and E. Ursino. Xmm-newton observations of the diffuse x-ray background. *The Astrophysical Journal*, 658(2):1081, 2007. URL `http://stacks.iop.org/0004-637X/658/i=2/a=1081`.

A. M. Garcia. General study of group membership. II - Determination of nearby groups. A&AS, 100:47–90, July 1993.

M. Gaspari, F. Brighenti, and P. Temi. Chaotic cold accretion on to black holes in rotating atmospheres. A&A, 579:A62, July 2015. doi: 10.1051/0004-6361/201526151.

P. C. Hanlan and J. N. Bregman. X-Ray Emission from Rotating Elliptical Galaxies. ApJ, 530:213–221, February 2000. doi: 10.1086/308357.

G. Hasinger, R. Burg, R. Giacconi, M. Schmidt, J. Trumper, and G. Zamorani. The ROSAT Deep Survey. I. X-ray sources in the Lockman Field. A&A, 329: 482–494, January 1998.

J. D. Hunter. Matplotlib: A 2d graphics environment. *Computing In Science & Engineering*, 9(3):90–95, 2007. doi: 10.1109/MCSE.2007.55.

J. A. Irwin, A. E. Athey, and J. N. Bregman. X-Ray Spectral Properties of Low-Mass X-Ray Binaries in Nearby Galaxies. ApJ, 587:356–366, April 2003. doi: 10.1086/368179.

F. Jansen, D. Lumb, B. Altieri, J. Clavel, M. Ehle, C. Erd, C. Gabriel, M. Guainazzi, P. Gondoin, R. Much, R. Munoz, M. Santos, N. Schartel, D. Texier, and G. Vacanti. XMM-Newton observatory. I. The spacecraft and operations. A&A, 365:L1–L6, January 2001. doi: 10.1051/0004-6361:20000036.

J. Ji, J. A. Irwin, A. Athey, J. N. Bregman, and E. J. Lloyd-Davies. Elemental Abundances in the X-Ray Gas of Early-Type Galaxies with XMM-Newton and Chandra Observations. ApJ, 696:2252–2268, May 2009. doi: 10.1088/0004-637X/696/2/2252.

C. Jones, W. Forman, E. Churazov, P. Nulsen, R. Kraft, and S. Murray. Cooling and feedback in galaxies and groups. In H. Böhringer, G. W. Pratt, A. Finoguenov, and P. Schuecker, editors, *Heating versus Cooling in Galaxies and Clusters of Galaxies*, pages 145–154. Springer-Verlag Berlin Heidelberg, 2007.

Eric Jones, Travis Oliphant, Pearu Peterson, et al. SciPy: Open source scientific tools for Python, 2001–. URL `http://www.scipy.org/`. [Online; accessed <today>].

J. S. Kaastra and J. A. M. Bleeker. Optimal binning of X-ray spectra and response matrix design. A&A, 587:A151, March 2016. doi: 10.1051/0004-6361/201527395.

J. S. Kaastra, R. Mewe, and H. Nieuwenhuijzen. SPEX: a new code for spectral analysis of X & UV spectra. In K. Yamashita and T. Watanabe, editors, *UV and X-ray Spectroscopy of Astrophysical and Laboratory Plasmas*, pages 411–414, 1996.

P. M. W. Kalberla, W. B. Burton, D. Hartmann, E. M. Arnal, E. Bajaja, R. Morras, and W. G. L. Pöppel. The Leiden/Argentine/Bonn (LAB) Survey of Galactic HI. Final data release of the combined LDS and IAR surveys with improved stray-radiation corrections. A&A, 440:775–782, September 2005. doi: 10.1051/0004-6361:20041864.

K. Lodders, H. Palme, and H.-P. Gail. Abundances of the Elements in the Solar System. *Landolt Börnstein*, 2009. doi: 10.1007/978-3-540-88055-4_34.

Malcolm S. Longair. *High Energy Astrophysics*. Cambridge University Press, 3 edition, 2011. ISBN 978-0-521-75618-1.

M. E. Machacek, E. O'Sullivan, S. W. Randall, C. Jones, and W. R. Forman. The Mysterious Merger of NGC 6868 and NGC 6861 in the Telescopium Group. ApJ, 711:1316–1332, March 2010. doi: 10.1088/0004-637X/711/2/1316.

W. G. Mathews and F. Brighenti. Hot Gas in and around Elliptical Galaxies. ARA&A, 41:191–239, 2003. doi: 10.1146/annurev.astro.41.090401.094542.

M. McCourt, P. Sharma, E. Quataert, and I. J. Parrish. Thermal instability in gravitationally stratified plasmas: implications for multiphase structure in clusters and galaxy haloes. MNRAS, 419:3319–3337, February 2012. doi: 10.1111/j.1365-2966.2011.19972.x.

B. R. McNamara and P. E. J. Nulsen. Heating Hot Atmospheres with Active Galactic Nuclei. ARA&A, 45:117–175, September 2007. doi: 10.1146/annurev.astro.45.051806.110625.

R. Mewe. Atomic Physics of Hot Plasmas. In J. van Paradijs and J. A. M. Bleeker, editors, *X-Ray Spectroscopy in Astrophysics*, volume 520 of *Lecture Notes in Physics, Berlin Springer Verlag*, page 109, 1999. doi: 10.1007/978-3-540-49199-6_2.

S. M. Moran, B. L. Loh, R. S. Ellis, T. Treu, K. Bundy, and L. A. MacArthur. The Dynamical Distinction between Elliptical and Lenticular Galaxies in Distant Clusters: Further Evidence for the Recent Origin of S0 Galaxies. ApJ, 665:1067–1073, August 2007. doi: 10.1086/519550.

A. Negri, S. Posacki, S. Pellegrini, and L. Ciotti. The effects of galaxy shape and rotation on the X-ray haloes of early-type galaxies - II. Numerical simulations. MNRAS, 445:1351–1369, December 2014. doi: 10.1093/mnras/stu1834.

P. E. J. Nulsen, G. C. Stewart, and A. C. Fabian. X-ray cooling flows in isolated elliptical galaxies. MNRAS, 208:185–195, May 1984. doi: 10.1093/mnras/208.2.185.

G. Paturel, P. Dubois, C. Petit, and F. Woelfel. Comparison LEDA/SIMBAD octobre 2002. Catalogue to be published in 2003. *LEDA, 0 (2002)*, 2002.

J. R. Peterson and A. C. Fabian. X-ray spectroscopy of cooling clusters. Phys. Rep., 427:1–39, April 2006. doi: 10.1016/j.physrep.2005.12.007.

S. Posacki, S. Pellegrini, and L. Ciotti. The effects of galaxy shape and rotation on the X-ray haloes of early-type galaxies. MNRAS, 433:2259–2274, August 2013. doi: 10.1093/mnras/stt898.

J. C. Raymond and B. W. Smith. Soft X-ray spectrum of a hot plasma. ApJS, 35:419–439, December 1977. doi: 10.1086/190486.

C. S. Reynolds, S. Heinz, and M. C. Begelman. Shocks and Sonic Booms in the Intracluster Medium: X-Ray Shells and Radio Galaxy Activity. ApJ, 549: L179–L182, March 2001. doi: 10.1086/319159.

Stephan Rosswog and Marcus Brüggen. *Introducton to High-Energy Astrophysics*. Cambridge University Press, 2007. ISBN 978-0-521-85769-7.

H. R. Russell, J. S. Sanders, and A. C. Fabian. Direct X-ray spectral deprojection of galaxy clusters. MNRAS, 390:1207–1216, November 2008. doi: 10.1111/j.1365-2966.2008.13823.x.

J. S. Sanders, A. C. Fabian, S. W. Allen, R. G. Morris, J. Graham, and R. M. Johnstone. Cool X-ray emitting gas in the core of the Centaurus cluster of galaxies. MNRAS, 385:1186–1200, April 2008. doi: 10.1111/j.1365-2966.2008.12952.x.

Peter Schneider. *Extragalactic Astronomy and Cosmology*. Springer, 2006. ISBN 978-3-540-33174-2.

K. M. Schure, D. Kosenko, J. S. Kaastra, R. Keppens, and J. Vink. A new radiative cooling curve based on an up-to-date plasma emission code. A&A, 508:751–757, December 2009. doi: 10.1051/0004-6361/200912495.

P. Sharma, M. McCourt, E. Quataert, and I. J. Parrish. Thermal instability and the feedback regulation of hot haloes in clusters, groups and galaxies. MNRAS, 420:3174–3194, March 2012. doi: 10.1111/j.1365-2966.2011.20246.x.

J. Shin, J.-H. Woo, and J. S. Mulchaey. A Systematic Search for X-Ray Cavities in Galaxy Clusters, Groups, and Elliptical Galaxies. ApJS, 227:31, December 2016. doi: 10.3847/1538-4365/227/2/31.

S. L. Snowden and K. D. Kuntz. Analysis of XMM-Newton Data from Extended Sources and the Diffuse X-ray Background. In *American Astronomical Society Meeting Abstracts #217*, volume 43 of *Bulletin of the American Astronomical Society*, page 344.17, January 2011.

S. L. Snowden, M. R. Collier, and K. D. Kuntz. XMM-Newton Observation of Solar Wind Charge Exchange Emission. ApJ, 610:1182–1190, August 2004. doi: 10.1086/421841.

L. Spitzer, Jr. and J. L. Greenstein. Continuous Emission from Planetary Nebulae. ApJ, 114:407, November 1951. doi: 10.1086/145480.

T. S. Statler and S. Diehl. Thermal structure of the hot ism in normal ellipticals: Evidence for local and distributed agn heating. In H. Böhringer, G. W. Pratt, A. Finoguenov, and P. Schuecker, editors, *Heating versus Cooling in Galaxies* *and Clusters of Galaxies*, pages 161–165. Springer-Verlag Berlin Heidelberg, 2007.

L. Strüder, U. Briel, K. Dennerl, R. Hartmann, E. Kendziorra, N. Meidinger, E. Pfeffermann, C. Reppin, B. Aschenbach, W. Bornemann, H. Bräuninger, W. Burkert, M. Elender, M. Freyberg, F. Haberl, G. Hartner, F. Heuschmann, H. Hippmann, E. Kastelic, S. Kemmer, G. Kettenring, W. Kink, N. Krause, S. Müller, A. Oppitz, W. Pietsch, M. Popp, P. Predehl, A. Read, K. H. Stephan, D. Stötter, J. Trümper, P. Holl, J. Kemmer, H. Soltau, R. Stötter, U. Weber, U. Weichert, C. von Zanthier, D. Carathanassis, G. Lutz, R. H. Richter, P. Solc, H. Böttcher, M. Kuster, R. Staubert, A. Abbey, A. Holland, M. Turner, M. Balasini, G. F. Bignami, N. La Palombara, G. Villa, W. Buttler, F. Gianini, R. Lainé, D. Lumb, and P. Dhez. The European Photon Imaging Camera on XMM-Newton: The pn-CCD camera. *Astrophys. J.*, 365:L18–L26, January 2001. doi: 10.1051/0004-6361:20000066.

J. L. Tonry, A. Dressler, J. P. Blakeslee, E. A. Ajhar, A. B. Fletcher, G. A. Luppino, M. R. Metzger, and C. B. Moore. The SBF Survey of Galaxy Distances. IV. SBF Magnitudes, Colors, and Distances. ApJ, 546:681–693, January 2001. doi: 10.1086/318301.

M. Tozuka and Y. Fukazawa. Heavy Element Analysis of X-Ray Faint Elliptical Galaxies. PASJ, 60:527–538, June 2008. doi: 10.1093/pasj/60.3.527.

W. H. Tucker and M. Koren. Radiation from a High-Temperature Low-Density Plasma: the X-Ray Spectrum of the Solar Corona. ApJ, 168:283, September 1971. doi: 10.1086/151083.

M. J. L. Turner, A. Abbey, M. Arnaud, M. Balasini, M. Barbera, E. Belsole, P. J. Bennie, J. P. Bernard, G. F. Bignami, M. Boer, U. Briel, I. Butler, C. Cara, C. Chabaud, R. Cole, A. Collura, M. Conte, A. Cros, M. Denby, P. Dhez, G. Di Coco, J. Dowson, P. Ferrando, S. Ghizzardi, F. Gianotti, C. V. Goodall, L. Gretton, R. G. Griffiths, O. Hainaut, J. F. Hochedez, A. D. Holland, E. Jourdain, E. Kendziorra, A. Lagostina, R. Laine, N. La Palombara, M. Lortholary, D. Lumb, P. Marty, S. Molendi, C. Pigot, E. Poindron, K. A. Pounds, J. N. Reeves, C. Reppin, R. Rothenflug, P. Salvetat, J. L. Sauvageot, D. Schmitt, S. Sembay, A. D. T. Short, J. Spragg, J. Stephen, L. Strüder, A. Tiengo, M. Trifoglio, J. Trümper, S. Vercellone, L. Vigroux, G. Villa, M. J. Ward, S. Whitehead, and E. Zonca. The European Photon Imaging Camera on XMM-Newton: The MOS cameras : The MOS cameras. A&A, 365:L27–L35, January 2001. doi: 10.1051/0004-6361:20000087.

Guido van Rossum. Python tutorial. Report CS-R9526, April 1995. URL `http://www.python.org/doc/tut/tut.html`.

G. M. Voit and M. Donahue. The Fate of Stellar Mass Loss in Central Cluster Galaxies. ApJ, 738:L24, September 2011. doi: 10.1088/2041-8205/738/2/L24.

G. M. Voit, K. W. Cavagnolo, M. Donahue, D. A. Rafferty, B. R. McNamara, and P. E. J. Nulsen. Conduction and the Star Formation Threshold in Brightest Cluster Galaxies. ApJ, 681:L5, July 2008. doi: 10.1086/590344.

N. Werner, A. Simionescu, E. T. Million, S. W. Allen, P. E. J. Nulsen, A. von der Linden, S. M. Hansen, H. Böhringer, E. Churazov, A. C. Fabian, W. R. Forman, C. Jones, J. S. Sanders, and G. B. Taylor. Feedback under the microscope-II. Heating, gas uplift and mixing in the nearest cluster core. MNRAS, 407: 2063–2074, October 2010. doi: 10.1111/j.1365-2966.2010.16755.x.

N. Werner, J. B. R. Oonk, M. Sun, P. E. J. Nulsen, S. W. Allen, R. E. A. Canning, A. Simionescu, A. Hoffer, T. Connor, M. Donahue, A. C. Edge, A. C. Fabian, A. von der Linden, C. S. Reynolds, and M. Ruszkowski. The origin of cold gas in giant elliptical galaxies and its role in fuelling radio-mode AGN feedback. MNRAS, 439:2291–2306, April 2014. doi: 10.1093/mnras/stu006.